NASA TECHNICAL NOTE

NASA TN D-8066

NASA TN D-8066

EXPERIMENTAL PARAMETRIC STUDIES OF TRANSONIC T-TAIL FLUTTER

Charles L. Ruhlin and Maynard C. Sandford

Langley Research Center
Hampton, Va. 23665

NATIONAL AERONAUTICS AND SPACE ADMINISTRATION • WASHINGTON, D. C. • DECEMBER 1975

1. Report No.	2. Government Accession No.	3. Recipient's Catalog No.
NASA TN D-8066		

4. Title and Subtitle	5. Report Date
EXPERIMENTAL PARAMETRIC STUDIES OF TRANSONIC T-TAIL FLUTTER	December 1975
	6. Performing Organization Code
7. Author(s)	8. Performing Organization Report No.
Charles L. Ruhlin and Maynard C. Sandford	L-10367
9. Performing Organization Name and Address	10. Work Unit No.
NASA Langley Research Center Hampton, Va. 23665	505-02-21-01
	11. Contract or Grant No.
12. Sponsoring Agency Name and Address	13. Type of Report and Period Covered
National Aeronautics and Space Administration Washington, D.C. 20546	Technical Note
	14. Sponsoring Agency Code

15. Supplementary Notes

16. Abstract

Wind-tunnel flutter studies of the T-tail of a wide-body jet airplane were made at Mach numbers up to 1.02. The model consisted of a 1/13-size scaled version of the T-tail, fuselage, and inboard wing of the airplane. Two interchangeable T-tails were tested, one with design stiffness for flutter-clearance studies and one with reduced stiffness for flutter-trend studies. Transonic antisymmetric-flutter boundaries were determined for the models with variations in (1) fin-spar stiffness, (2) stabilizer dihedral angle $\left(-5^{\circ}\right.$ and $\left.0^{\circ}\right)$, (3) wing and forward-fuselage shape, and (4) nose shape of the fin-stabilizer juncture. A transonic symmetric-flutter boundary and flutter trends were established for variations in stabilizer pitch stiffness.

17. Key Words (Suggested by Author(s))	18. Distribution Statement
Flutter Transonic speeds T-tails	Unclassified – Unlimited Subject Category 39

19. Security Classif. (of this report)	20. Security Classif. (of this page)	21. No. of Pages	22. Price*
Unclassified	Unclassified	50	$3.75

*For sale by the National Technical Information Service, Springfield, Virginia 22161

EXPERIMENTAL PARAMETRIC STUDIES OF TRANSONIC T-TAIL FLUTTER

Charles L. Ruhlin and Maynard C. Sandford
Langley Research Center

SUMMARY

Flutter studies of the T-tail of a wide-body, multijet, cargo/transport airplane have been conducted in the Langley transonic dynamics tunnel at Mach numbers up to 1.02. The flutter model was a 1/13-size scaled version of the empennage, fuselage, and inboard wing of the airplane. Two interchangeable T-tails were used. One had scaled design stiffnesses and control surfaces (elevator and rudder). The second T-tail had about one-half the scaled design stiffnesses and the control-surface area made integral with the primary surfaces.

The transonic antisymmetric-flutter boundary for this T-tail was unusual in that over half of the total transonic drop in flutter speed occurred in a sharp dip between a Mach number M of 0.92 and 0.98. This result necessitated tests of the design-stiffness model with a stiffened fin spar in order to demonstrate a greater margin of safety from flutter. Parametric studies of the reduced-stiffness model were made to determine a possible cause of this unusual flutter boundary shape, as well as to establish flutter trends. The sharp drop in flutter speed near $M = 0.92$ was at least reduced and may have been eliminated by modifying the shape of the fin-stabilizer juncture fairing. The modification consisted of adding a bulbous-shaped section near the nose of the streamlined juncture fairing so that a sharper peak in the empennage cross-sectional area distribution was obtained.

Transonic antisymmetric-flutter boundaries were determined for the reduced-stiffness model with variations in (1) the stabilizer dihedral angle $\left(-5^{\circ}\right.$ (nominal) and $\left.0^{\circ}\right)$, and (2) the wing and forward-fuselage shape. Limited antisymmetric-flutter tests were made at $M = 0.7$ to determine the effect of varying stabilizer incidence angle. A transonic symmetric-flutter boundary was determined with a reduced stabilizer pitch stiffness, and flutter trends were established for variations in stabilizer pitch stiffness at $M = 0.7$ and 0.8.

INTRODUCTION

Several aerodynamic theories have been developed for predicting subsonic and supersonic flutter of nonplanar and interacting lifting surfaces such as T-tails (e.g., see ref. 1). However, at transonic Mach numbers, where flutter speeds are generally the lowest and most critical to high-speed aircraft designs, complex shock patterns significantly affect the interacting flow fields about such surfaces and make flutter analyses difficult and uncertain. Experimental flutter data are needed by aircraft designers to estimate transonic Mach number effects and

to correlate with analysis. However, available experimental T-tail flutter data are limited, particularly for antisymmetric flutter. The purpose of this paper is to present some additional experimental trends on transonic T-tail flutter.

Reported herein are the results of a transonic flutter investigation of the T-tail of a wide body, multijet, cargo/transport airplane. A number of transonic flutter studies of T-tail models of a similar but smaller airplane (refs. 2 to 4) had generated considerable data on symmetric flutter but little data on antisymmetric flutter. The emphasis in the present studies was to establish the transonic shape of the antisymmetric-flutter-speed boundary and to provide design trends for both antisymmetric and symmetric flutter. The flutter experiments were conducted in the Langley transonic dynamics tunnel in Freon-12 at Mach numbers from about 0.4 to 1.02.

The models used in the present investigation were 1/13-size with the T-tail, fuselage, and inboard portion of the wing geometrically, dynamically, and elastically scaled. Two different, interchangeable models of the T-tail (comprising the horizontal and vertical tail) were flutter tested. One model represented the nominal design stiffness and included the elevators and rudders. The purpose of the design-stiffness model was to provide flutter-clearance data. It was found that the antisymmetric-flutter-speed boundary for this T-tail had an unusual and unexpected shape at transonic speeds, resulting in a flutter boundary very close to the airplane flutter-clearance envelope. In order to demonstrate a greater margin of safety, the design-stiffness model was also tested with a stiffened fin spar.

In an effort to determine the cause of the unusual transonic antisymmetric-flutter boundary as well as to determine parametric trends, a second T-tail model having roughly one-half the nominal design stiffnesses and having the control-surface area integral with the main tail surfaces was tested. This reduced-stiffness model was investigated with (1) the stabilizer dihedral angle increased from -5° to 0°, (2) a change in the wing and forward-fuselage shape (in order to reduce the aerodynamic interference on the T-tail from these surfaces), and (3) an altered nose shape of the fin-stabilizer juncture fairing (in order to obtain a sharper peak in the empennage cross-sectional area distribution). These parameters were selected with a view of matching the present model more closely to the test conditions of the model of reference 3. Following the antisymmetric studies, the effects of varying stabilizer pitch stiffness on the symmetric-flutter characteristics of the reduced-stiffness model were investigated.

SYMBOLS

Values are presented in both SI and U.S. Customary Units. The measurements and calculations were made in U.S. Customary Units.

b_f fin semichord at fin root, 0.3627 m (1.190 ft)

b_s stabilizer semichord at plane of symmetry, 0.2444 m (0.8017 ft)

EI bending stiffness, kN-m^2 $\left(\text{lbf-in}^2\right)$

f_e natural frequency of elevator rotation, Hz

f_f flutter frequency, Hz

f_m natural frequency of horizontal-tail pitch mode for complete model (see table V(b)), Hz

f_p natural frequency of horizontal-tail pitch mode for empennage cantilevered at fin root (see table V(b)), Hz

f_r natural frequency of rudder rotation, Hz

f_t natural frequency of fin first-torsion mode for empennage cantilevered at fin root, Hz

f_θ uncoupled pitch frequency of horizontal tail, $\frac{1}{2\pi}\sqrt{\frac{K_\theta}{I_\theta}}$, Hz

GJ torsional stiffness, kN-m^2 $\left(\text{lbf-in}^2\right)$

g structural damping coefficient

I_{ea} mass moment of inertia of stabilizer section or fin section about its elastic axis, kg-m^2 $\left(\text{slug-ft}^2\right)$

I_{hl} mass moment of inertia of elevator or rudder about its hinge axis, kg-m^2 $\left(\text{slug-ft}^2\right)$

I_θ mass moment of inertia of forward fin-stabilizer juncture fairing and enclosed stabilizer or complete horizontal tail (including elevators and forward portion of fin-stabilizer juncture fairing) in pitch about horizontal-tail pivot axis, kg-m^2 $\left(\text{slug-ft}^2\right)$

I_ϕ mass moment of inertia of horizontal tail (including elevators and forward portion of fin-stabilizer juncture fairing) in roll about intersection of stabilizer horizontal plane and plane of symmetry, kg-m^2 (slug-ft^2)

I_ψ mass moment of inertia of horizontal tail (including elevators and forward portion of fin-stabilizer juncture fairing) in yaw about a vertical axis through intersection of fin elastic axis and stabilizer horizontal plane, kg-m^2 (slug-ft^2)

K_θ horizontal-tail pitch-spring stiffness, m-N/rad (in-lbf/rad)

M Mach number

m_e total mass of empennage, kg (slugs)

m_h total mass of horizontal tail (including elevators and forward portion of fin-stabilizer juncture fairing). For configurations D1 and D1-s, m_h = 2.798 kg (0.1917 slug); for configurations R1, R1-d, R1-w, R2, R3, and R4, m_h = 2.345 kg (0.1606 slug); for configuration R1-b, m_h = 2.571 kg (0.1762 slug)

m_v total mass of vertical tail (including rudder and aft portion of fin-stabilizer juncture fairing), kg (slugs)

q dynamic pressure, kN/m^2 (lbf/ft^2)

N_{Re} Reynolds number per unit length, m^{-1} (ft^{-1})

S_{ea} mass unbalance of stabilizer section or fin section about its elastic axis, kg-m (slug-ft)

S_{hl} mass unbalance of elevator or rudder about its hinge axis, kg-m (slug-ft)

V free-stream velocity, m/s (ft/sec)

v volume of a conical frustum having horizontal-tail root chord as base diameter, horizontal-tail tip chord as upper diameter, and horizontal-tail semispan as height, 0.1495 m^3 (5.28 ft^3)

α_F angle of attack of fuselage measured at model center of gravity, deg

a_s angle of attack of horizontal stabilizer, deg

δ_s incidence angle of horizontal stabilizer relative to the reference stabilizer chord plane, deg

η nondimensional distance along elastic axis (spar center line) of fin or stabilizer measured from elastic-axis root, fraction of elastic-axis length

μ mass-density ratio of horizontal tail, $m_h/2\rho v$

ρ test-medium density, kg/m^3 $\left(slugs/ft^3\right)$

Subscript:

o nominal design condition

Abbreviations:

BL buttock line, cm (in.)

FS fuselage station, cm (in.)

WL water line, cm (in.)

MODELS

General Description

The basic model used in this investigation was a 1/13-size version of a wide-body, multijet, cargo/transport airplane. Sketches and photographs of the basic model and modifications are presented in figures 1 and 2. Some geometric properties are listed in table I along with those of a T-tail flutter model (ref. 3) which had been extensively flutter tested. Note that the two models have many similar properties, the major exceptions being the horizontal-tail dihedral angle and the taper ratio of the vertical tail.

The T-tail, fuselage, and inboard wing of the present model (figs. 1(a) and 2(a)) were geometrically, dynamically, and elastically scaled in an effort to simulate the Mach number, mass ratio, and reduced frequency of the airplane in the atmosphere with the model in Freon. As constructed, the models were considerably overweight. Consequently, at the flutter clearance envelope, the mass-density ratio and reduced frequency for the model were about 2.48

and 1.81 times, respectively, those for the airplane. The outboard wing and engine nacelles of the airplane were represented on the model by a single mass on each wing tip so that the first two vibration modes of the airplane wing were roughly simulated.

Two different, interchangeable models of the T-tail were used and are designated as design-stiffness empennage and reduced-stiffness empennage (figs. 1(b) and 1(c)). The design-stiffness empennage represented the nominal design stiffnesses for the complete model and included elevators and rudders (fig. 2(c)). The reduced-stiffness empennage represented about one-half the nominal design stiffness of only the horizontal tail and vertical tail and had control-surface area integral with the primary surfaces (fig. 2(d)).

The model configurations investigated are listed in table II. The model configurations have been divided into two groups, those that used the design-stiffness empennage (table II(a)) and those that used the reduced-stiffness empennage (table II(b)). For simplicity, the model configurations have been given coded designations. In this code, the letter D or R indicates that a design-stiffness empennage or a reduced-stiffness empennage, respectively, was used. Following this is a number that indicates the horizontal-tail pitch spring used. When present, the letters b, d, s, or w indicate a variation from the nominal condition. For example, the R1-d configuration represented the reduced-stiffness empennage with pitch spring 1, and differed from the nominal condition by having a stabilizer dihedral angle of 0° instead of the nominal -5°.

The design-stiffness empennage configurations (table II(a)) consisted of the nominal design configuration (D1) and the final design configuration (D1-s) which had a stiffened fin spar. The reduced-stiffness empennage configurations (table II(b)) consisted of the basic nominal configuration (R1) and of modified R1 configurations with a dihedral angle of 0° (R1-d), with a change in the wing and forward-fuselage shape (R1-w), and with a change in the shape of the fin-stabilizer juncture fairing (R1-b), and also of configurations with various weakened stabilizer pitch springs (R2, R3, and R4).

Construction

The model was built using a spar-and-pod technique. In each component, a single metal spar provided the required bending and torsional stiffnesses and lightweight pine and balsa pods gave the required shape. The balsa contour sections were covered with doped silk span. Lead weights were glued in the pods to yield the required mass and inertia properties. Gaps between the pods were aerodynamically sealed with sponge rubber. The construction technique was similar to that for the model of reference 3.

Stabilizer and fin.- Two different, interchangeable T-tail models were constructed, a design-stiffness and a reduced-stiffness model. The stabilizer and fin are shown in figures 1(b) and 1(c). Note that in the typical sectional areas of the reduced-stiffness empennage there are no separate control surfaces and also that the spars were different in cross section from

those of the design-stiffness model. The tubular spars of the reduced-stiffness model proved to be very durable for flutter testing. The stiffer-than-design fin spar (spar S) used with the D1-s configuration was similar in cross section to the twin-cell, box-type spar used with the design-stiffness model (fig. 1(c)).

The stabilizer was attached to the vertical tail by two aluminum bracket arms with self-alining, ball-bearing pivots which fitted on a lateral shaft mounted at the top of the fin spar. The stabilizer could be remotely trimmed in pitch relative to the fin (i.e., vary δ_s by means of a jack screw driven through an articulated shaft by an electric motor located in the fuselage (see figs. 1(c) and 1(d))). The jack screw was attached to the stabilizer through an interchangeable metal bar spring (the stabilizer pitch spring) which simulated the stiffness of the pitch-trim actuator. A number of these springs of various stiffnesses were available. The stabilizer dihedral angle was changed from -5° to 0° by inserting a wedge between the left and right stabilizer spars at the spar juncture.

The fin-stabilizer junction area was enclosed by a fairing of balsa wood covered with doped silk. The aft portion of the fairing was attached to the upper fin airfoil section and the forward portion was attached to and moved with the stabilizer. (In constrast, the fairing on the model of ref. 3 was attached entirely to the horizontal tail.) The gap between the forward and rear sections of the fairing was sealed with flexible tape. For one configuration (R1-b), an additional bulbous section of hollow balsa was added to the fairing nose (fig. 2(d)). The added nose section was symmetrical about the fairing longitudinal axis and had a maximum diameter of about 16.5 cm (6.5 in.).

Control surfaces.- Split control surfaces were used on the design-stiffness empennage. The elevator and rudder spars were constructed of a thin metal tube surrounded by balsa which formed the leading edge of the control. The contours were built up of pine and balsa ribs covered with doped Japanese tissue. Control-surface rotational stiffnesses were obtained by use of leaf spring flexures (figs. 1(b) and 1(c)). Only the outboard elevators were mass balanced.

Fuselage and wings.- The fuselage had a tubular aluminum spar with the pod skin and bulkheads made of balsa and pine (figs. 1(a) and 1(d)). The model fuselage spar scaled the vertical bending, lateral bending, and torsional stiffness of the airplane fuselage (fig. 3(a)). The stub wings were built with an aluminum spar and with the outer skin and ribs of balsa wood. An aluminum plate about 2.5 cm (1 in.) thick was mounted on each wing tip and simulated the mass properties of the outer wing and engine nacelles on the airplane.

For the reduced-stiffness configuration R1-w (fig. 2(b)), the contours of the fuselage forward of the wing, the wing airfoils, and the wing-tip plate were removed. A balsa nose section was installed in the fuselage spar and a balsa section was built to provide a faired surface from the fuselage spar to the forward section of the remaining fuselage. Concentrated weights were added to give the same overall model center of gravity. Wooden wedges were

added to the leading and trailing edges of the wing spars and the spar and wedges wrapped with fiberglass cloth to reduce the drag of the bare spar. The wing-tip mass was replaced by a strut and beam having about the same mass and inertial properties.

Mounting cage.- The model was mounted in the center of the tunnel on a mounting cage supported by steel cables (fig. 1(d)). Vertical translation motion of the model was permitted by springs located in the upper and lower mounting cables but exterior to the test section. The mounting cage was made of aluminum and consisted of an upper and lower plate joined by a yoke that extended around the fuselage spar (fig. 1(d)). The model fuselage was attached to the cage by four lengths of 0.478-cm (0.188-in.) diameter music wire with one upper and one lower wire clamped at each of two points on the fuselage about the center of gravity. These four music wires supported the model and allowed limited motion in pitch, fore-and-aft translation, yaw, roll, and side translation. Springs were attached between the yoke and the fuselage spar to relieve the drag loads on the wires. With the exception of the upper and lower cable mounting posts, the entire cage was enclosed within the model fuselage contours (figs. 1(a) and 2(a)).

Instrumentation

Electric resistance-wire strain gages were mounted near the root of the stabilizer, fin, and wing spars to indicate static and oscillatory deflections in bending and torsion. Strain gages were also mounted on the rudder and elevator rotation springs to indicate angular deflections. Nominal stabilizer incidence angles were measured by potentiometers connected to the actuator drive motors. In determining the stabilizer incidence angle, static deflections of the pitch spring and fin structure were not accounted for but were considered not to be significant. Strain gages were attached to the aft-fuselage spar in order to indicate deflections in vertical bending, lateral bending, and torsion. An inclinometer and an accelerometer were mounted near the model center of gravity to determine the fuselage pitch angle and vertical translational motion, respectively. All electrical leads were combined into a single umbilical cord and carried down the lower mounting cable. Tufts of yarn were attached to the surfaces of the vertical and horizontal tail for flow visualization (figs. 2(c) and 2(d)).

Physical Properties

Mass and stiffness.- Mass and stiffness properties of the model configurations are given in tables III and IV and in figure 3. The model configurations D1 and D1-s have the same mass properties. All the reduced-stiffness configurations (R-series) have the same mass properties with the exception of R1-b which had the added nose section on the fin-stabilizer juncture fairing. The stiffnesses of the various stabilizer pitch springs (table IV) were measured separately from the model and therefore do not include the flexibility of the pitch actuator or model structure.

Vibration frequencies and node lines.- Presented in table V(a) are the antisymmetric- and symmetric-mode natural frequencies for the complete model mounted in the tunnel and for the empennages cantilevered at the fin root. Nodal patterns associated with these frequencies are shown in figure 4.

The R1 and D1 empennages were originally designed to be basically similar except for stiffness level. Therefore, the two models would be expected to have similar vibration modes but different frequency levels. In order to show how closely the two models are related, the frequencies of the R1 model have been adjusted to account for this difference in stiffness level (and also mass differences that occurred in construction) by multiplying each R1 model frequency by the ratio of the fin first-torsion frequencies for the D1 and R1 models $\left(\text{Ratio} = \frac{10.2}{9.0} = 1.13\right)$. Although this frequency adjustment factor is lower than would be predicted based on the reduction in fin-spar stiffness alone (the R1 model has about one-half the stiffness of the D1 model (fig. 3(b)), the horizontal tail of the R1 model was also considerably lighter and had lower inertias (table III(a)) than the D1 model. These adjusted frequencies are included in table V for both the complete model and the cantilevered model. It can be seen that for most of the primary modes the R1 model matches the D1 model fairly well.

Only a limited number of modes for the D1-s model were measured. It was surprising to find that the increase in torsional stiffness of the fin spar between the D1 and D1-s models was not reflected in the fin torsion frequencies measured for the complete models. In contrast, the cantilevered-model frequencies increased as expected. For this reason, the fin torsion frequencies for the cantilevered condition were used in normalizing the antisymmetric-flutter results.

Of the R1-series model configurations, only the frequencies of the basic R1 model were actually measured, and the remaining models in that series were assumed to have the same frequencies. An attempt was made to isolate and measure the frequency of the stabilizer pitch mode for the various pitch springs and the results are shown in table V(b) and are also included in figure 11.

APPARATUS AND TESTS

Tunnel

The studies were conducted in the Langley transonic dynamics tunnel which has a 4.88-m-square (16-ft) test section (with cropped corners). The tunnel is a return-flow, slotted-throat wind tunnel. It is a variable-pressure tunnel and can be operated at stagnation pressures from near vacuum to slightly above atmospheric and at Mach numbers from 0 to 1.2. Mach number and dynamic pressure can be varied independently with either air or Freon-12 (dichlorodifluoromethane) used as a test medium. The present study was made using

Freon. The tunnel is equipped with four quick-opening bypass valves which can be opened when flutter occurs in order to reduce rapidly the dynamic pressure and Mach number in the test section.

Mount System

The model was supported in the tunnel by a cable-spring system so that the model rigid-body frequencies were low relative to the T-tail structural vibration modes considered important to flutter. Photographs of the model in the tunnel are shown in figures 2(a) and 2(b), and a sketch of the mounting system is shown in figure 1(d). The model was supported in the tunnel by cables which were attached to the upper and lower posts of the mounting cage described previously (see section entitled "Models"). Springs in cables 1 and 2 (fig. 1(d)) allowed freedom of the model in vertical translation whereas flexure of the four vertical music wires which connected the model fuselage to the mounting cage permitted model motion in roll, pitch, yaw, and lateral and longitudinal translation. Drag loads on the music wires were relieved by two springs which connected the side plates of the mounting cage to the fuselage (fig. 1(d)) and also by a continuous cable (cable 7) which extended forward from the model. Exterior to the test section, cable 7 passed between friction plates which were used to provide damping in yaw to the model. Also used but not shown in figure 1(d) were four vertical cables (snubbers) which were used to restrain the model in the center of the tunnel. These cables were attached top and bottom near the front and aft end of the fuselage spar. The snubbers were normally slack during testing and were engaged in emergency situations such as unusually violent flutter. They were also engaged during the tests to measure the effects of stabilizer incidence angle on flutter in an attempt to restrain the fuselage at a nearly constant angle of attack.

Tests

Equipment.- During the tests, strain-gage and accelerometer signals from the model were continuously recorded on direct readout recorders and magnetic tape. Visual records of model and tuft behavior were provided by high-speed motion pictures taken from the sides and from the rear. The tunnel test conditions, stabilizer incidence angle, and fuselage angle of attack were digitized and printed automatically. The purity of the Freon varied during the tests between 88 to 96 percent by volume (97 to 99 percent by weight).

Procedure.- Prior to testing, the model angle of attack α_F and the stabilizer incidence angle δ_S were nominally 0^o. During the test as the dynamic pressure was increased, the model tended to rise in the tunnel because of lift on the wing sections. This was counteracted by trimming with the horizontal tail. The test procedure that evolved represented a compromise between keeping the loads and angle changes on the stabilizer to a minimum, while keeping the model within reasonable position limits in the tunnel. For one model

configuration, the stabilizer incidence angle was purposely varied about 2° to determine its effect on the antisymmetric-flutter speed while attempting to maintain a constant fuselage angle of attack by engaging the snubber cables.

The tests were limited to Mach numbers less than 1.02 which was sufficient to cover the transonic dip in flutter speed as well as to exceed the design limit of the airplane. The test dynamic pressures were limited to less than 7.2 kN/m^2 $\left(150\ lbf/ft^2\right)$ for model structural safety.

The test procedure was to set a given stagnation pressure in the tunnel and vary the Mach number (and dynamic pressure) from a low subsonic value up to conditions where the model fluttered or the limit Mach number (or limit dynamic pressure) was reached. At flutter, the bypass valves were opened to reduce quickly the dynamic pressure and Mach number in the test section. The stagnation pressure of each Mach number sweep was varied successively from a low value up to higher values until the flutter boundary was sufficiently defined or until the limit dynamic pressure was reached without flutter. Basic model frequencies were checked periodically to insure against visually undetected model damage. The present test procedure was similar to that described in reference 3.

RESULTS AND DISCUSSION

Presentation of Results

The experimental results of the present studies are compiled in table VI, and some of the results are plotted in figures 5 to 11. In figures 6, 7, and 10 the results are presented as the variations with Mach number of the basic nondimensional flutter parameters which include mass-density ratio μ, the flutter frequency ratio f_f/f_t $\left(\text{or } f_f/f_p\right)$, and the flutter-speed index $\frac{V}{b_f\left(2\pi f_t\right)\sqrt{\mu}}$ $\left(\text{or } \frac{V}{b_s\left(2\pi f_p\right)\sqrt{\mu}}\right)$. The nondimensional flutter-speed index is used to correlate data obtained with models of different stiffness and/or mass levels. The flutter-speed-index curves represent stability boundaries, with the stable region (no flutter) below the curves. In forming these nondimensional parameters, the reference frequencies used were those measured for the cantilevered model because they best reflected the variations in the fin-spar torsional stiffnesses and stabilizer pitch-spring stiffnesses. The mass-density ratio μ values were formed using the horizontal-tail mass and its enclosed volume. (See μ, m_h, and v in the Symbols.)

Antisymmetric-Flutter Studies

General comments.- The antisymmetric flutter of the present model configurations involved primarily fin bending and torsion with accompanying stabilizer bending and yaw. The flutter frequencies were between the natural vibration frequencies of the fin first-bending and fin first-torsion modes. Generally, the flutter was preceded by a short period of low damping and

rapidly built up to large amplitudes. In one instance, the flutter amplitudes were sufficiently large to cause a permanent bend and twist in the fin spar of a reduced-stiffness configuration. The spar was subsequently straightened and reused successfully. This type of spar construction proved to be very durable for flutter testing.

It is known that the stabilizer angle of attack, and hence static aerodynamic loads on the horizontal tail, may have an appreciable effect on a T-tail antisymmetric flutter speed. For example, low-speed wind-tunnel tests of other T-tails (refs. 3, 5, and 6) indicated a 4 to 6 percent reduction in flutter speed per degree increase in stabilizer angle of attack. The stabilizer angle of attack α_S obtained by summing the fuselage angle of attack α_F and the stabilizer incidence angle δ_S is given in table VI. These tabulated α_S values show only a small variation for each configuration because a change in δ_S was largely offset by a change in α_F in the opposite direction.[1] Therefore, although stabilizer angle of attack is recognized as an important parameter in antisymmetric flutter, it is not accounted for in the subsequent discussion of the present results. In the present tests, an attempt was made to maintain a constant stabilizer incidence angle (2°) for most of the antisymmetric-flutter points except those for the R1-w configuration, which had no wing airfoil sections. Limited tests were made to evaluate the effect of stabilizer incidence angle and are discussed in a subsequent section.

Basic configurations.- In figure 5, the experimental flutter boundaries obtained for model configurations D1, D1-s, and R1 are compared with the airplane flutter clearance envelope (i.e., the envelope required to be demonstrated as free from flutter). The boundaries are shown as the variation with Mach number of the dynamic pressures required for flutter. Experimental no-flutter points are included as an aid in defining the flutter boundaries. Note that the flutter-boundary dip near $M = 0.92$ of the nominal design T-tail configuration D1 lies very close to the airplane clearance envelope. Because this flutter-boundary dip could conceivably occur at slightly lower Mach numbers for the airplane T-tail and thus fall within the clearance envelope, a new fin spar, stiffened in torsion by about 33 percent, was designed and tested. This model configuration, D1-s, was shown (fig. 5) to have ample flutter clearance. As expected, the reduced-stiffness model R1 had a much lower flutter boundary.

At Mach numbers less than 0.92, all three model configurations had what is considered typical experimental transonic-flutter boundaries, that is, the flutter dynamic pressures progressively decreased with increasing Mach number. However, above $M = 0.92$ all three flutter boundaries dropped sharply to a minimum near $M = 0.98$. For the R1 model, the flutter dynamic pressure decreased about 44 percent from $M = 0.92$ to 0.98, and sizable but less percentage drops of about 40 percent and 25 percent were indicated for the D1 and D1-s models, respectively. (These percentage drops for the D1 and D1-s models were based on the no-flutter

[1]The actual stabilizer angle of attack was, of course, also affected by the aft-fuselage bending slope, the wing downwash, and the fin aerodynamic interference. Therefore, the α_S values in table VI are only roughly representative values.

points and are the maximum possible values.) It was this unusual dip that necessitated the stiffer fin spar (and thus heavier airplane tail weight) to clear this T-tail design.

The basic nondimensional flutter parameters for these configurations are plotted in figure 6. The overall transonic drop in flutter speed varied from a 29-percent to less than a 25-percent reduction in flutter speed from the low-speed (M = 0.7) value. The plot of the flutter frequency ratio f_f/f_t shows that a slight shift in the modal coupling at flutter for the D1-s model may have occurred, possibly the result of increasing only the fin torsional stiffness. In spite of this and the variations in mass ratio μ of the three models, there is good agreement in the Mach number trend of the flutter-speed index $\left(\frac{V}{b_f(2\pi f_t)\sqrt{\mu}}\right)$, and the steep dip at M = 0.92 is still very evident.

One factor that should be considered in interpreting the present unusual flutter boundary is possible wind-tunnel-wall interference. In reference 7, flutter speeds of wall-mounted models were shown to have been affected by model size and some model-to-tunnel size limits for transonic flutter testing were recommended. The present empennage is within those recommended limits but the complete model, which includes wings and fuselage as well, was somewhat oversize. Using the complete-model-size parameters, a crude estimate of tunnel-wall effects on flutter was made based on reference 8 and the estimated correction to the subsonic flutter speed was about 1 percent which was within the experimental scatter of the present tests. Tunnel-wall interference would be expected to have a gradually increasing effect as sonic speed was approached (refs. 7 and 8) and, therefore, was not likely to have caused a sharp dip in flutter speed such as that obtained with the present T-tail at $M \approx 0.92$.

Reference 7 also shows that when the tunnel acoustic-resonance frequencies are near a model flutter frequency, the tunnel resonances can affect the flutter speeds in a closed (slots-sealed) tunnel but have no apparent effect in a ventilated (slots-open) tunnel such as the present test facility. Admittedly, the present antisymmetric-flutter frequencies are within the range of tunnel acoustic-resonance frequencies predicted for the present slotted tunnel with Freon at Mach numbers from 0.92 to 0.95 (ref. 7). However, based on the above considerations and past experience with other transonic flutter models, the tunnel resonances are not believed to affect significantly the present model results.

Because of the similarity in planform between the present model and the T-tail model of reference 3 (see table I), it had been expected that the antisymmetric-flutter boundaries would also be somewhat similar. A comparison of the normalized flutter boundaries for this previously tested model and the present R1 model is presented in figure 8(b), and it may be seen that the boundary shapes differ significantly. In an effort to determine the possible cause of the unusual shape of the present-model flutter boundary, as well as to establish additional flutter design trends, a number of geometric variations were studied which were related to matching more closely the present model to that of reference 3. Flutter studies were made with the reduced-stiffness model having (1) an increased stabilizer dihedral angle from

-5° to 0°, (2) an altered wing and forward-fuselage shape, and (3) an altered nose shape of the fin-stabilizer juncture fairing. In the following discussions the results for each parametric change are compared with the basic R1 model results.

Effects of varying stabilizer dihedral and incidence angles.- By a relatively simple structural change, the stabilizer dihedral angle on the reduced-stiffness empennage was increased from -5° to 0° to form the R1-d configuration. The results (fig. 7(a)) show that the R1-d configuration had the same general transonic-flutter-boundary shape as the basic R1 configuration. For equal stabilizer incidence angles $\left(\delta_s \approx 2^{\circ}\right)$, increasing the stabilizer dihedral angle from -5° to 0° decreased the flutter speed about 10 percent at the lower subsonic Mach numbers. This effect agrees qualitatively with other T-tail flutter experiments and calculations (refs. 6 and 9 to 12). At $M > 0.92$, however, the dihedral angle had little or no effect on the flutter speeds, and the same sharp dip in flutter speed was obtained.

An attempt was made to evaluate the effect of stabilizer incidence angle on the flutter. At each of the two lowest subsonic flutter points, the stabilizer incidence angle was changed from 2° to 0°, and the model tested to flutter. The snubber cables, which were attached to the front and rear of the fuselage, were also engaged for these test points in an effort to prevent any fuselage rotation in pitch. Unfortunately, the snubbers proved to be ineffective and each change in stabilizer incidence angle was offset by a change in fuselage trim angle (see table VI(a)). Nevertheless, when the stabilizer incidence was changed from 2° to 0°, the actual stabilizer lift was decreased and the flutter speed increased about 2 percent for each degree decrease in stabilizer incidence angle. Because any stabilizer-angle change was effectively reduced by the accompanying fuselage-angle change, the actual effect of stabilizer incidence angle would be greater than the measured 2 percent per degree.

Effects of varying wing shape and forward-fuselage shape.- The wing and forward-fuselage shapes of the basic R1 model were altered (fig. 2(b)) to resemble the model of reference 3. Removal of the forward-fuselage contours and wing airfoil sections is believed to have reduced substantially any aerodynamic interference from these surfaces on the T-tail.

The test results for this configuration (R1-w) are shown in figure 7(b), and, in general, the flutter trends were similar to those for the basic R1 model but the R1-w model fluttered at higher speeds at the lower subsonic Mach numbers. These higher subsonic flutter speeds are at least partially due to the differences in the stabilizer incidence angles between the two tests since with the forward-fuselage contours and wing airfoil sections removed, the model required lower stabilizer incidence angles for trim (table VI(a)). After accounting for these incidence-angle differences using the measured results for the R1-d model, the R1-w model still appears to have slightly higher (about 3 or 4 percent) flutter speeds than the R1 model at the lower subsonic Mach numbers. However, the sharp dip in flutter speed near $M = 0.92$ remained basically unchanged.

Effects of varying fin-stabilizer juncture shape.- The R1-b model configuration consisted of the basic R1 model with a bulbous-shaped section added to the nose of the streamlined fin-stabilizer juncture fairing. The basic and altered fairing shapes are shown in figures 2(c) and 2(d).

The new fairing shape was designed from the following considerations. It was observed (fig. 8(a)) that the empennage area distribution (cross-sectional area taken normal to the longitudinal axis) for the model of reference 3 was more peaked than that for the present model. To obtain a sharper peak in the area distribution for the present model that could be made simply and quickly, an additional bulbous section was designed and built on the nose of the fin-stabilizer juncture fairing. The resulting area distribution is shown in figure 8(a).

The test results (fig. 7(c)) show that this fairing change at least reduced and may have eliminated the dip in flutter speed beyond $M = 0.92$. This dip in flutter speed amounted to a 24 percent decrease from the value at $M = 0.92$ for the R1 model as compared with a maximum dip of 13 percent for the R1-b model based on the no-flutter points. At the subsonic Mach numbers, however, the R1-b model fluttered at lower speeds.

The flutter-speed index was normalized by the value at $M = 0.4$ for the R1 and R1-b models and the resulting boundaries are presented in figure 8(b) along with that for the T-tail model of reference 3. (For this comparison, the normalized boundary for the R1 model was formed from a straight-line extrapolation to $M = 0.4$ of the flutter-speed-index boundary presented in the bottom plot of fig. 6.) The comparison shows the basically different transonic boundary shapes between the present R1 model and the model of reference 3. Note that the boundary for the R1-b model appears to be somewhat of a mean between the other two boundaries with a considerably reduced overall transonic drop in flutter speed.

Thus, although the subsonic flutter speeds were reduced, the overall effect of the fairing change on the flutter was favorable because the minimum transonic flutter speed was raised considerably (fig. 7(c)). Also, the overall transonic drop in flutter speed was much less with the fairing change (fig. 8(b)). The present altered fairing shape may be unacceptable from an aerodynamic point of view; nevertheless, area distribution of the empennage and especially of the juncture fairing may be a promising subject of future flutter studies.

Symmetric-Flutter Studies

General comments.- Symmetric-flutter studies were made of three model configurations, designated R2, R3, and R4, which consisted of the basic reduced-stiffness empennage with three different stabilizer pitch springs having less-than-nominal pitch stiffness. The transonic shape of the symmetric-flutter boundary was defined with the R3 configuration and limited tests were made with both a stiffer (R2) and weaker (R4) pitch spring to establish flutter trends. The experimental results are compiled in table VI(b) and plotted in figures 9 to 11.

Included in these plots are two points selected from the antisymmetric data for the R1-w model to indicate no-symmetric-flutter points for the nominal stabilizer pitch stiffness.

Transonic-flutter-boundary shape.- A symmetric-flutter boundary was established for the R3 configuration (fig. 9) and indicates that the dynamic pressure q required for flutter decreased at least 60 percent as the Mach number increased from 0.4 to 0.82, with the minimum flutter q near $M = 0.82$. The equivalent drop in flutter-speed index was about 34 percent (fig. 10). Note that values of the mass-density ratio μ for the R3 configuration vary considerably over the Mach number range (fig. 10). Since the symmetric flutter speed of a T-tail is a function of mass ratio, especially at low μ-values (see ref. 2), this large drop in flutter speed is probably caused by the variations in mass ratio as well as in Mach number.

Limited results obtained with the R2 and R4 configurations indicate the flutter-boundary shapes for these configurations are probably similar to that for the R3 model with minimum flutter speeds also near $M = 0.82$ (fig. 9). However, the data for the three spring stiffnesses were not correlated well by the flutter-speed index (fig. 10). These differences may be caused by a shifting in the structural mode coupling at flutter as suggested by the spread in the f_f/f_p ratios, although such a shift was not visually detected. The symmetric flutter for all models appeared to involve stabilizer pitching, stabilizer bending, and to a lesser extent aft-fuselage vertical bending.

Effect of varying stabilizer pitch stiffness.- The experimental results show (fig. 9) that, as expected, increasing the pitch stiffness raised the symmetric-flutter dynamic pressure. The effects of varying the stabilizer pitch-spring stiffness K_θ on the flutter q and related model vibration frequencies are shown in figure 11. The flutter dynamic pressures used in this plot were obtained from the curves and no-flutter data of figure 9 at Mach numbers of 0.7 and 0.8. The trends indicate that the flutter q varies nearly linearly with pitch stiffness up to the higher stiffness values. However, the stabilizer pitch frequencies for the cantilevered model f_p and for the complete model f_m do not follow the expected uncoupled frequency f_θ trend above certain stiffness levels. This leveling off in f_p and f_m was attributed to either reaching an effective pitch stiffness level which was limited by the flexibility in the pitch drive system or the result of some unusual modal coupling so that a new low-frequency vibration mode was identified as the stabilizer pitch mode. The flutter frequencies f_f also appear to level off similarly to the f_m curve, but no such effect was noted in the flutter q which continued to increase up to the highest stiffness level tested.

CONCLUSIONS

Flutter studies of the T-tail of a wide-body, multijet, cargo/transport airplane have been conducted in the Langley transonic dynamics tunnel at Mach numbers M up to 1.02. The flutter model was a 1/13-size, scaled version of the empennage, fuselage, and inboard wing

portion of the airplane. Two interchangeable T-tails were used; namely, a design-stiffness model having scaled control surfaces, and a reduced-stiffness model having about one-half the scaled nominal stiffnesses with control-surface area made integral with the primary surfaces.

The antisymmetric-flutter results of the T-tail models tested with various parametric changes indicate the following conclusions:

1. The antisymmetric-flutter-speed boundaries were similar for the design-stiffness model, the design-stiffness model with a stiffened fin spar, and the basic reduced-stiffness model. The overall transonic drop in the flutter-speed boundaries of these models varied from a 29-percent to less than a 25-percent reduction from the low-speed ($M = 0.7$) value, with the minimum flutter speed occurring near $M = 0.98$.

2. Over half of the total transonic drop in the antisymmetric-flutter-speed boundaries occurred in an unusual sharp dip between $M = 0.92$ and 0.98. On one model configuration, this dip was at least reduced and may have been eliminated by the addition of a bulbous-shaped section to the streamlined aerodynamic fairing enclosing the fin-stabilizer juncture so as to provide a sharper peak in the cross-sectional area distribution of the empennage. Area-distribution effects on T-tail antisymmetric flutter appear to be a promising subject for future study.

3. Changing the dihedral angle of the horizontal tail from -5° (nominal) to 0° decreased the antisymmetric flutter speeds at the lower subsonic Mach numbers but had little effect at the higher Mach numbers. At $M = 0.7$, decreasing the horizontal-tail incidence angle from 2° to 0° increased the flutter speed at least about 2 percent per degree.

4. Removing the wing airfoil sections and forward-fuselage contours (leaving essentially only the structural spars) in order to reduce the aerodynamic interference from these surfaces on the T-tail increased slightly the antisymmetric flutter speeds at the lower subsonic Mach numbers.

The symmetric-flutter results of the T-tail model tests with reduced stiffness of the stabilizer pitch spring indicate these additional conclusions:

5. The symmetric-flutter-speed boundary indicated a reduction in flutter speed of about 34 percent from the low-speed ($M = 0.4$) value, with the minimum flutter speed occurring near $M = 0.82$. This large reduction in flutter speed is probably caused by the variations in model mass-density ratio as well as in Mach number.

6. Flutter trends were established showing the effect of varying stabilizer pitch stiffness. The results indicate the dynamic pressure required for symmetric flutter increases nearly linearly with stabilizer pitch stiffness and at about the same rate at $M = 0.7$ and 0.8.

Langley Research Center
National Aeronautics and Space Administration
Hampton, Va. 23665
October 23, 1975

REFERENCES

1. Symposium on Unsteady Aerodynamics for Aeroelastic Analyses of Interfering Surfaces. Part I and II. AGARD-CP-80-71, Apr. 1971.
2. Ruhlin, Charles L.; Sandford, Maynard C.; and Yates, E. Carson, Jr.: Wind-Tunnel Flutter Studies of the Sweptback T-Tail of a Large Multijet Cargo Airplane at Mach Numbers to 0.90. NASA TN D-2179, 1964.
3. Sandford, Maynard C.; Ruhlin, Charles L.; and Yates, E. Carson, Jr.: Subsonic and Transonic Flutter and Flow Investigations of the T-Tail of a Large Multijet Cargo Airplane. NASA TN D-4316, 1968.
4. Sandford, Maynard C.; and Ruhlin, Charles L.: Wind-Tunnel Study of Deflected-Elevator Flutter Encountered on a T-Tail Airplane. NASA TN D-5024, 1969.
5. McCue, D. J.; Gray, R.; and Drane, D. A.: The Effect of Steady Tailplane Lift on the Subcritical Response of a Subsonic T-Tail Flutter Model. R. & M. No. 3652, British A.R.C., 1971.
6. Jennings, W. P.; and Berry, M. A.: The Flutter Analysis of T-Tails. AIAA Paper No. 75-759, May 1975.
7. Ruhlin, Charles L.; Destuynder, Roger M.; and Gregory, Richard A.: Some Tunnel-Wall Effects on Transonic Flutter. J. Aircr., vol. 12, no. 3, Mar. 1975, pp. 162-167.
8. Garner, H. C.; Moore, A. W.; and Wight, K. C.: The Theory of Interference Effects on Dynamic Measurements in Slotted-Wall Tunnels at Subsonic Speeds and Comparisons With Experiment. R. & M. No. 3500, British A.R.C., 1968.
9. Goldman, R. L.: Flutter of T-Tails With Dihedral. ER 8205, Martin Co., 1957.
10. Land, Norman S.; and Fox, Annie G.: An Experimental Investigation of the Effects of Mach Number, Stabilizer Dihedral, and Fin Torsional Stiffness on the Transonic Flutter Characteristics of a Tee-Tail. NASA TN D-924, 1961. (Supersedes NACA RM L57A24.)
11. Kobayashi, Shigeo: The State of the Art in Aeroelasticity of Aerospace Vehicles in Japan. AIAA Paper No. 73-331, Mar. 1973.
12. Washizu, K.; IchiKawa, T.; and Adachi, T.,(D. Jackson, Transl): A Note on the T-Tail Flutter. Transl. No. 1546, British R.A.E., Apr. 1971.

TABLE I.- GEOMETRIC PROPERTIES

	Present model[a]	Model of ref. 3
Horizontal tail:		
Stabilizer with elevator:		
Aspect ratio	4.74	5.22
Sweepback angle of quarter-chord line, deg	24.6	25
Taper ratio	0.37	0.37
Airfoil section (streamwise)	NACA 0010.5 (modified)	NACA 64A010
Dihedral angle (negative tip down), deg	-5.0	0.0
Mean aerodynamic chord, m (ft)	0.359 (1.18)	0.350 (1.15)
Elastic-axis location, fraction of horizontal-tail local chord (streamwise)	0.32	0.40
Pitch pivot-axis, fraction of horizontal-tail chord at BL 0.0 (streamwise)	0.59	0.60
Elevator:		
Number per side	2	1
Exposed area, fraction of horizontal-tail area	0.27	0.23
Hinge axis, fraction of horizontal-tail local chord (streamwise)	0.66	0.75
Vertical tail:		
Fin with rudder:		
Aspect ratio	1.24	1.24
Sweepback angle of quarter-chord line, deg	34.9	35
Taper ratio	0.80	0.61
Airfoil section (streamwise)	NACA 0013 (modified)	NACA 64A012
Mean aerodynamic chord, m (ft)	0.656 (2.15)	0.632 (2.07)
Elastic-axis location, fraction of vertical-tail local chord (streamwise)	0.37	0.39
Rudder:		
Number	2	1
Exposed area, fraction of vertical-tail area	0.24	0.20
Hinge axis, fraction of vertical-tail local chord (streamwise)	0.71	0.77

[a]Control-surface area made integral with main surface for present reduced-stiffness empennage configurations.

TABLE II.- SUMMARY OF MODEL CONFIGURATIONS INVESTIGATED

(a) Design-stiffness empennage configurations

Configuration (a)	Fin spar (b)	Stabilizer			Rudder				Inboard elevators				Outboard elevators			
		Spar	Pitch spring	f_θ, Hz	Upper		Lower		Left		Right		Left		Right	
					f_r, Hz	g	f_r, Hz	g	f_e, Hz	g	f_e, Hz	g	f_e, Hz	g	f_e, Hz	g
D1	D	D	1	58.9	81.9	0.055	41.6	0.130	95.7	0.037	83.5	0.080	112.5	0.056	113.2	0.046
D1-s	S	D	1	58.9	← Assumed same as D1 configuration →											

(b) Reduced-stiffness empennage configurations having control-surface area integral with main surfaces

Configuration (a)	Fin spar (c)	Stabilizer spar (c)	Test variables					Comments
			Stabilizer			Shape of wing and fuselage	Shape of stabilizer-fin juncture fairing	
			Pitch spring	f_θ, Hz	Dihedral, deg			
R1	R	R	1	65.8	−5	Nominal	Nominal	Basic reduced-stiffness configuration.
R1-d	↓	↓	↓	↓	0	Nominal	↓	Reduced stabilizer dihedral angle to 0°.
R1-w	↓	↓	↓	↓	−5	Altered	↓	Altered wing and forward-fuselage shapes.
R1-b	↓	↓	↓	50.1	−5	Nominal	Altered	Altered nose shape of stabilizer-fin juncture fairing.
R2	R	R	2	58.7	−5	Nominal	Nominal	} Reduced stiffness of stabilizer pitch spring.
R3	↓	↓	3	37.2	↓	↓	↓	
R4	↓	↓	4	27.2	↓	↓	↓	

[a] D indicates design-stiffness empennage configuration; R indicates reduced-stiffness empennage configuration. The number designates pitch spring used; s indicates variation in fin-spar stiffness; d, stabilizer dihedral angle; w, altered wing and forward-fuselage shape; and b, altered stabilizer-fin fairing shape.

[b] Fin spar S is stiffer than spar D in overall GJ and EI by about 33 and 7 percent, respectively.

[c] Fin spar R and stabilizer spar R are roughly one-half as stiff as corresponding spar D in both overall GJ and EI.

TABLE III.- MASS PROPERTIES OF MODEL CONFIGURATIONS

(a) Major model components

Total model (configuration D1):		
Mass, kg (slugs)	120.28	(8.242)
Center of gravity, cm (in.)	FS 268.0	(105.5)
Fuselage mass, kg (slugs)	55.57	(3.808)
Wing and tip weight:		
Wing mass (full span), kg (slugs)	17.50	(1.199)
Tip-weight mass (both sides), kg (slugs)	36.29	(2.487)
Inertia in roll about fuselage center line, kg-m^2 (slug-ft^2)	64.69	(47.714)
Empennage (configuration D1):		
Total empennage mass, $m_{e,o}$, kg (slugs)	5.455	(0.374)
Vertical-tail mass[a], $m_{v,o}$, kg (slugs)	2.657	(0.182)
Horizontal tail[b]:		
Mass, $m_{h,o}$, kg (slugs)	2.798	(0.192)
Center of gravity, cm (in.)	FS 567.7	(223.5)
Center of gravity, cm (in.) (estimated)	WL 153.7	(60.5)
$I_{\theta,o}$, kg-m^2 (slug-ft^2)	0.0596	(0.044)
$I_{\psi,o}$, kg-m^2 (slug-ft^2)	0.3783	(0.279)
$I_{\phi,o}$, kg-m^2 (slug-ft^2)	0.3634	(0.268)

Configuration	$m_e/m_{e,o}$	$m_v/m_{v,o}$	Horizontal tail (b)					
			Center of gravity		$m_h/m_{h,o}$	$I_\theta/I_{\theta,o}$	$I_\psi/I_{\psi,o}$	$I_\phi/I_{\phi,o}$
			FS, cm	FS, in.				
D1, D1-s	1.000	1.000	567.7	223.5	1.000	1.000	1.000	1.000
R1, R1-d, R1-w, R2, R3, R4	.936	1.041	568.4	223.8	.838	.802	.860	.821
R1-b	.978	1.041	565.2	222.5	.919	1.385	.932	.830

[a]Includes aft portion of stabilizer-fin juncture fairing.

[b]Includes full-span horizontal stabilizer, elevators, and forward stabilizer juncture fairing.

TABLE III.- MASS PROPERTIES OF MODEL CONFIGURATIONS - Continued

(b) Typical component mass distributions

Fuselage				
Section	Section limits		Mass	
	FS, cm	FS, in.	kg	slugs
1	Nose to 66.42	Nose to 26.15	1.982	0.1358
2	66.42 to 97.69	26.15 to 38.46	3.034	.2079
3	97.69 to 127.00	38.46 to 50.00	4.650	.3186
4	127.00 to 156.21	50.00 to 61.50	2.817	.1930
5	156.21 to 185.60	61.50 to 73.07	2.485	.1703
6	185.60 to 224.69	73.07 to 88.46	6.196	.4246
7	224.69 to 266.70	88.46 to 105.00	10.042	.6881
8	266.70 to 296.93	105.00 to 116.90	7.357	.5041
9	296.93 to 327.30	116.90 to 128.86	4.731	.3242
10	327.30 to 352.68	128.86 to 138.85	2.332	.1598
11	352.68 to 378.05	138.85 to 148.84	1.788	.1225
12	378.05 to 404.44	148.84 to 159.23	2.010	.1377
13	404.44 to 429.84	159.23 to 169.23	1.702	.1166
14	429.84 to 457.20	169.23 to 180.00	1.456	.0998
15	457.20 to 488.47	180.00 to 192.31	1.179	.0808
16	488.47 to 519.71	192.31 to 204.61	1.239	.0849
17	519.71 to Tail	204.61 to Tail	.572	.0392
Total	Nose to tail	Nose to tail	55.569	3.8079

Forward fin-stabilizer juncture fairing and enclosed stabilizer						
Configuration	Center of gravity		Mass		I_0	
	FS, cm	FS, in.	kg	slugs	kg-m^2	slug-ft^2
D1, D1-s	553.2	217.8	0.897	0.0615	17.57×10^{-3}	12.96×10^{-3}
R1, R1-d, R1-w, R2, R3, R4	554.9	218.4	.658	.0451	17.96	13.25
R1-b	548.8	216.0	.885	.0606	46.67	34.42

TABLE III.- MASS PROPERTIES OF MODEL CONFIGURATIONS – Concluded

(b) Typical component mass distributions – Concluded

Section	Section limit, η	Configuration D1 (no control surfaces)						Configuration R1 (integral control-surface area)					
		Mass		S_{ea}		I_{ea}		Mass		S_{ea}		I_{ea}	
		kg	slugs	kg-m	slug-ft	kg-m^2	slug-ft^2	kg	slugs	kg-m	slug-ft	kg-m^2	slug-ft^2
Fin													
1	0.0 to 0.0808	0.278	0.0190	1.092×10^{-3}	0.245×10^{-3}	4.039×10^{-3}	2.979×10^{-3}	0.508	0.0348	8.105×10^{-3}	1.822×10^{-3}	7.942×10^{-3}	5.858×10^{-3}
2	0.0808 to 0.2492	.355	.0243	-3.744	-.842	5.961	4.397	.408	.0280	13.436	3.020	11.226	8.280
3	0.2492 to 0.4175	.309	.0212	2.083	.468	3.710	2.736	.369	.0253	6.193	1.392	7.606	5.610
4	0.4175 to 0.5858	.291	.0199	-2.522	-.567	3.555	2.622	.344	.0236	7.214	1.622	7.619	5.620
5	0.5858 to 0.7542	.300	.0206	.140	.0315	2.681	1.977	.342	.0234	11.328	2.547	8.284	6.110
6	0.7542 to 1.0	.908	.0622	24.613	5.53	39.919	29.443	.794	.0544	31.628	7.110	15.277	11.268
Total	0.0 to 1.0	2.441	0.167	----------	----------	----------	----------	2.765	0.189	----------	----------	----------	----------
Stabilizer (semispan)													
1	0.0833 to 0.2435	0.184	0.0126	2.983×10^{-3}	0.671×10^{-3}	1.290×10^{-3}	0.951×10^{-3}	0.230	0.0158	11.107×10^{-3}	2.497×10^{-3}	3.348×10^{-3}	2.469×10^{-3}
2	0.2435 to 0.4037	.142	.0097	-.643	-.144	.806	.594	.185	.0127	7.267	1.634	1.961	1.446
3	0.4037 to 0.5639	.130	.0089	2.672	.601	.508	.375	.149	.0102	4.511	1.014	1.245	.918
4	0.5639 to 0.7241	.135	.0092	.759	.171	.361	.266	.133	.0091	3.558	.800	.735	.542
5	0.7241 to 0.8869	.082	.0056	.053	.0119	.211	.156	.103	.0070	.607	.136	.331	.244
6	0.8869 to 1.0	.033	.0023	.309	.0074	.116	.0855	.043	.0029	.632	.142	.110	.0811
Total	0.0 to 1.0	0.706	0.0484	----------	----------	----------	----------	0.843	0.0578	----------	----------	----------	----------

Control surfaces (configuration D1)							
Surface	Mass balance, percent	Mass		S_{ht}		I_{ht}	
		kg	slugs	kg-m	slug-ft	kg-m^2	slug-ft^2
Lower rudder	0	0.1182	0.0081	4.694×10^{-3}	1.055×10^{-3}	0.486×10^{-3}	0.358×10^{-3}
Upper rudder	0	.0974	.0067	3.955	.889	.377	.278
Inboard elevator[a]	0	.0885	.0061	1.930	.434	.190	.140
Outboard elevator[a]	100	.1560	.0107	.117	.0263	.160	.118

[a]Per semispan.

TABLE IV.- STIFFNESSES OF STABILIZER PITCH SPRINGS AND FIN-STABILIZER JOINTS

(a) Pitch-spring stiffness

Spring	Pitch stiffness, K_θ	
	m-N/rad	in-lbf/rad
1	8160	72 200
2	6480	57 400
3	2610	23 100
4	1390	12 300
[a]5	670	5 930

(b) Fin-stabilizer-joint stiffness[b]

Fin spar	Yaw due to yawing moment		Yaw due to rolling moment (c)		Roll due to yawing moment (c)		Roll due to rolling moment	
	m-N/rad	in-lbf/rad	m-N/rad	in-lbf/rad	m-N/rad	in-lbf/rad	m-N/rad	in-lbf/rad
D	13 160	116 500	-45 190	-400 000	-779 600	-6 900 000	13 100	116 000
R	12 550	111 100	-67 800	-600 000	72 885	645 000	17 910	158 500
S	Not measured, assumed same as spar D							

[a]Not tested, used in vibration survey only.

[b]Stiffnesses were measured between station on fin elastic axis at WL 145 cm (57.1 in.) and the point on underside of stabilizer spar at elastic axis where bracket arm is attached. Sign convention of deflections and applied moments:

Positive roll, right stabilizer tip downward.

Positive yaw, right stabilizer tip rearward.

[c]In determining cross-coupled stiffness values the measured deflections were very small and probably affected by measurement scatter.

TABLE V.- MEASURED NATURAL FREQUENCIES OF MODEL CONFIGURATIONS

(a) Basic model configurations

Vibration mode (a)	Frequency, Hz, of –							
	Complete model				Cantilevered model (at fin root)			
	R1		D1 measured	D1-s measured	R1		D1 measured	D1-s measured
	Measured	Scaled to D1 configuration (b)			Measured	Scaled to D1 configuration (b)		
Antisymmetric modes								
Complete model yaw	1.50	-----	0.92	-----	-----	-----	-----	-----
Complete model roll	.67	-----	.54	-----	-----	-----	-----	-----
Complete model lateral translation	1.67	-----	3.39	-----	-----	-----	-----	-----
Aft-fuselage torsion	5.2	5.9	-----	-----	-----	-----	-----	-----
Fin first bending	5.7	6.4	6.3	[c]7.3	6.3	7.4	6.7	7.5
Fin first torsion	9.0	10.2	10.2	[c]10.3	9.2	10.4	10.4	11.8
Stabilizer yaw, fuselage lateral bending	11.4	12.9	12.3	-----	14.0	15.8	15.4	16.6
	-----	-----	12.7	-----	-----	-----	-----	-----
Wing torsion, stabilizer yaw	-----	-----	14.3	-----	-----	-----	-----	-----
Fuselage lateral bending, fin bending, stabilizer yaw	14.5	16.4	16.4	-----	-----	-----	-----	-----
Fuselage lateral bending and torsion, fin bending and torsion	15.7	17.7	-----	-----	-----	-----	-----	-----
Stabilizer roll	21.5	24.3	24.5	-----	-----	-----	-----	24.1
Stabilizer first bending and roll, fin bending and torsion	27.8	31.4	30.0	-----	14.6 54.3	16.4 61.5	48.0	-----
Stabilizer first bending	-----	-----	-----	-----	-----	-----	49.7	-----
Fuselage lateral bending, stabilizer bending and yaw	43.0	48.5	45.6	-----	-----	-----	-----	-----
Stabilizer pitch, fuselage lateral bending, fin torsion	-----	-----	65.3	-----	63.0	71.0	60.5	-----
	-----	-----	79.3	-----	66.2	74.9	-----	-----
Stabilizer bending	-----	-----	88.3	-----	-----	-----	-----	-----
	-----	-----	[d]96.7	-----	-----	-----	-----	-----
Elevator rotation, stabilizer torsion	-----	-----	104.0	-----	-----	-----	95.0	-----
Stabilizer bending	-----	-----	-----	-----	106.0	119.0	117.0	-----
Symmetric modes								
Complete model pitch	2.18	-----	1.88	None measured	-----	-----	-----	None measured
Complete model vertical translation	1.33	-----	1.18	↓	-----	-----	-----	↓
Complete model fore and aft translation	3.0	-----	3.09		-----	-----	-----	
Wing first bending	-----	-----	7.4		-----	-----	-----	
Wing bending and torsion, fuselage vertical bending	10.1	11.4	10.6		-----	-----	-----	
Wing torsion, fuselage vertical bending, fin fore and aft	-----	-----	15.5		-----	-----	14.6	
Stabilizer first bending, fuselage vertical bending	16.9	19.1	21.3		19.2	21.6	22.9	
Fuselage vertical bending, stabilizer bending	21.8	24.6	23.3		-----	-----	-----	
Stabilizer bending, wing bending	-----	-----	30.0		-----	-----	-----	
Stabilizer torsion or pitch, fuselage vertical bending	-----	-----	51.3		-----	-----	61.5	
	-----	-----	69.0		-----	-----	-----	
Stabilizer bending, elevator rotation, fuselage bending	-----	-----	75.0		-----	-----	74.5	
Stabilizer torsion or pitch, fuselage bending	68.0	76.6	87.5		66.0	74.5	66.5	

[a]Where response in more than one degree of freedom is given, the underlined item is believed to be the primary degree of freedom.

[b]Scaled to D1 configuration by the ratio of fin-torsion frequencies, Ratio = 10.2/9.0 (or 10.42/9.2) = 1.13.

[c]Node lines same as for D1 configuration.

[d]No node lines measured.

TABLE V.- MEASURED NATURAL FREQUENCIES OF MODEL CONFIGURATIONS – Concluded

(b) Reduced-stiffness configuration with various pitch springs

Vibration mode	Model configuration	f_θ, Hz	f_p, Hz	f_m, Hz
Stabilizer pitch	[a]R5	18.5	26.5	---
↓	R4	27.2	34.7	32
	R3	37.2	48.0	46
	R2	58.7	66.0	46
	R1	65.8	66.0	---

[a]Pitch spring 5 was used in vibration survey only and not tested.

TABLE VI.- COMPILATION OF TEST RESULTS

(a) Antisymmetric-flutter configurations

Model configuration	Run point	Model behavior (a)	M	q		V		ρ		N_{Re}		f_F, Hz	f_f/f_t	μ	$\frac{V}{b_f(2\pi f_t)\sqrt{\mu}}$	α_F, deg	δ_s, deg	α_s, deg
				kN/m^2	lbf/ft^2	m/sec	ft/sec	kg/m^3	$slug/ft^3$	1/m	1/ft							
D1	1-1	NF	0.958	3.22	67.3	146.4	480.4	0.300	0.000583	3.48×10^6	1.06×10^6	-----	-----	62.2	0.783	2.5	0.0	2.5
	-2	F-A	.942	4.67	97.5	144.7	474.9	.446	.000865	5.05	1.54	8.00	0.769	42.0	.942	1.5	2.0	3.5
	-3	F-A	.923	5.73	118.9	142.0	465.8	.568	.001096	6.27	1.91	8.65	.832	33.1	1.041	1.7	2.0	3.7
	-4	F-A	.871	5.97	124.6	134.4	441.0	.660	.001281	6.92	2.11	8.37	.805	28.3	1.066	.7	2.0	2.7
	-5	F-A	.808	6.40	133.7	124.7	409.2	.823	.001597	7.97	2.43	8.68	.835	22.7	1.104	.5	2.0	2.5
	-6	F-A	.742	6.88	143.6	114.9	376.9	1.042	.001022	9.25	2.82	8.65	.832	18.0	1.143	.3	2.0	2.3
	-7	NF	.627	6.91	144.4	97.3	319.3	1.460	.002833	10.92	3.33	-----	-----	12.8	1.148	.2	2.0	2.2
D1-s	2-1	NF	1.012	5.53	115.5	153.4	503.2	.470	.000912	5.77	1.76	-----	-----	39.8	.904	1.2	1.8	3.0
	-2	NF	.966	5.19	109.0	147.1	482.5	.480	.000936	5.64	1.72	-----	-----	38.8	.878	1.3	1.8	3.1
	-3	F-A	.939	6.65	139.0	142.6	467.8	.654	.001270	7.45	2.27	8.21	.696	28.6	.992	1.3	1.8	3.1
	-4	F-A	.911	7.67	160.3	138.5	454.4	.800	.001553	8.83	2.69	8.32	.705	23.4	1.065	1.2	2.0	3.2
	-5	F-A	.772	9.42	197.0	117.9	386.9	1.356	.002632	12.63	3.85	9.45	.801	13.8	1.180	-.5	2.1	1.6
R1	3-1	NF	1.015	2.19	45.6	158.1	518.8	.175	.000339	2.13	.65	-----	-----	89.7	.796	1.9	.2	2.1
	-2	F-A	.972	2.54	53.1	148.7	487.9	.230	.000446	2.72	.83	7.02	.763	68.2	.859	1.2	2.0	3.2
	-3	F-A	.950	2.75	57.5	147.1	482.6	.254	.000494	2.89	.88	7.08	.770	61.6	.894	1.0	1.9	2.9
	-4	F-A	.939	2.93	61.2	144.4	473.6	.281	.000546	3.18	.97	7.50	.815	55.7	.923	1.0	1.9	2.9
	-5	F-A	.934	3.23	67.5	144.9	475.5	.308	.000597	3.44	1.05	7.13	.775	51.0	.968	1.0	1.9	2.9
	-6	F-A	.917	4.27	89.1	141.7	464.8	.425	.000825	4.69	1.43	7.28	.791	36.9	1.123	1.3	2.0	3.4
	-7	F-A	.688	4.99	104.3	105.1	344.7	.904	.001755	7.51	2.29	7.69	.836	17.3	1.205	1.3	1.9	3.3
R1-d	4-1	NF	.998	2.21	46.1	154.5	506.8	.185	.000359	2.23	.68	-----	-----	84.7	.801	1.4	1.8	3.2
	-2	F-A	.953	2.67	55.9	147.7	484.6	.245	.000476	2.79	.85	7.84	.852	63.9	.881	1.3	1.8	3.1
	-3	F-A	.931	3.17	66.4	144.9	475.5	.302	.000587	3.38	1.03	7.35	.799	51.8	.960	1.4	1.8	3.2
	-4	F-A	.907	4.08	85.4	141.3	463.7	.409	.000794	4.43	1.35	7.41	.805	38.3	1.089	1.4	1.9	3.3
	-5	F-A	.727	4.19	87.5	113.2	371.3	.654	.001269	5.71	1.74	7.78	.846	24.0	1.102	1.2	1.9	3.1
	-6	F-A	.749	4.39	91.8	116.5	382.3	.647	.001256	5.81	1.77	7.56	.822	24.2	1.130	3.2	.0	3.2
	-7	F-A	.634	4.39	91.7	98.8	324.2	.899	.001745	6.82	2.08	7.89	.858	17.4	1.130	.8	2.1	2.9
	-8	F-A	.663	4.75	99.1	103.3	338.9	.890	.001726	7.05	2.15	7.79	.847	17.6	1.174	3.0	.2	3.2
R1-w	5-1	NF	1.015	2.24	46.9	154.5	506.9	.188	.000365	2.30	.70	-----	-----	83.3	.807	.9	.0	.9
	-2	F-A	.984	2.46	51.6	150.0	492.0	.220	.000426	2.62	.80	6.83	.742	71.4	.847	.7	.0	.7
	-3	F-A	.950	3.17	66.3	145.1	476.1	.301	.000585	3.48	1.06	7.20	.783	52.0	.960	.5	.0	.5
	-4	F-A	.933	3.75	78.3	142.8	468.4	.368	.000714	4.17	1.27	7.31	.795	42.6	1.044	.4	.1	.5
	-5	F-A	.750	5.53	115.5	116.1	380.8	.821	.001593	7.38	2.25	7.65	.832	19.1	1.267	.1	.0	.1
	-6	F-A	.423	7.13	148.6	65.0	213.1	3.374	.006546	17.06	5.20	8.60	.935	4.6	1.446	.0	-1.0	-1.0
R1-b	6-1	NF	.911	2.86	59.8	138.8	455.4	.297	.000577	3.28	1.00	-----	-----	57.8	.871	.1	1.8	1.9
	-2	NF	1.016	3.31	69.1	154.2	505.8	.278	.000540	3.44	1.05	-----	-----	61.8	.936	.8	1.8	2.6
	-3	F-A	.940	4.15	86.6	143.1	469.5	.405	.000786	4.62	1.41	7.43	.808	42.4	1.048	.5	1.8	2.3
	-4	F-A	.764	4.31	90.0	117.1	384.3	.628	.001219	5.77	1.76	7.65	.832	27.4	1.067	.0	1.8	1.8
	-5	F-A	.647	4.53	94.7	99.6	326.9	.914	.001773	7.12	2.17	7.69	.836	18.8	1.096	-.2	1.7	1.5
	-6	F-A	.432	6.02	125.6	66.4	217.7	2.732	.005300	14.14	4.31	7.82	.850	6.2	1.272	-.6	1.8	1.2

(b) Symmetric-flutter configurations

Model configuration	Run point	Model behavior (a)	M	q		V		ρ		N_{Re}		f_F, Hz	f_f/f_p	μ	$\frac{V}{b_s(2\pi f_p)\sqrt{\mu}}$	α_F, deg	δ_s, deg	α_s, deg
				kN/m^2	lbf/ft^2	m/sec	ft/sec	kg/m^3	$slug/ft^3$	1/m	1/ft							
R4	7-1	NF	0.864	2.06	43.1	132.8	435.7	0.234	0.000454	2.43×10^6	0.74×10^6	-----	-----	67.0	0.305	0.9	0.1	1.0
	-2	NF	.908	2.21	46.2	139.3	457.0	.228	.000442	2.49	.76	-----	-----	68.8	.316	1.1	.1	1.2
	-3	F-S	.754	2.26	47.2	116.5	382.2	.333	.000647	3.02	.92	17.6	0.507	47.0	.319	.7	.1	.8
R3	8-1	F-S	.814	2.63	54.9	125.5	411.7	.334	.000648	3.28	1.00	21.3	.444	46.9	.249	1.3	.1	1.4
	-2	F-S	.706	3.04	63.3	109.1	357.9	.510	.000989	4.33	1.32	21.7	.452	30.8	.267	1.3	.1	1.4
	-3	F-S	.540	4.16	86.8	83.2	272.9	1.201	.002330	7.78	2.37	22.0	.458	13.0	.314	1.9	.1	2.0
	-4	NF	.402	6.30	131.6	61.3	201.2	3.352	.006504	16.08	4.90	-----	-----	4.7	.384	2.2	.1	2.3
R2	9-1	NF	.900	4.19	87.9	137.1	449.9	.446	.000866	4.86	1.48	-----	-----	35.1	.229	2.3	.1	2.4
	-2	F-S	.789	4.36	91.0	120.9	396.8	.596	.001156	5.68	1.73	22.8	.346	26.3	.233	2.1	.0	2.1
	-3	F-S	.720	4.67	97.6	110.8	363.7	.761	.001476	6.59	2.01	23.3	.353	20.6	.241	1.9	.1	2.0

[a]Model-behavior code: NF, no flutter; F-A, empennage flutter in antisymmetric mode; and F-S, empennage flutter in symmetric mode.

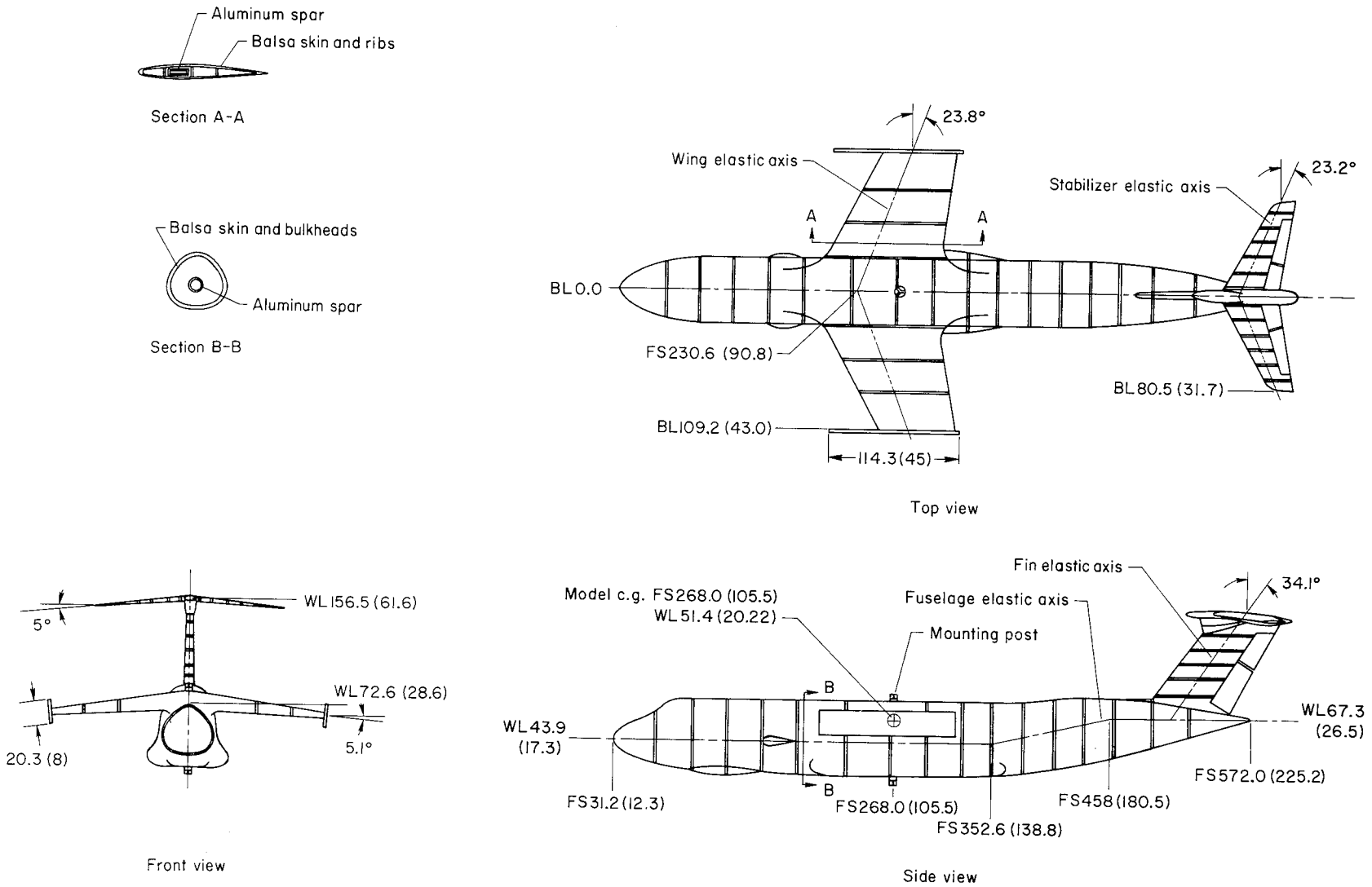

(a) Complete model.

Figure 1.- Sketches of model. All dimensions are in cm (in.) except as noted otherwise.

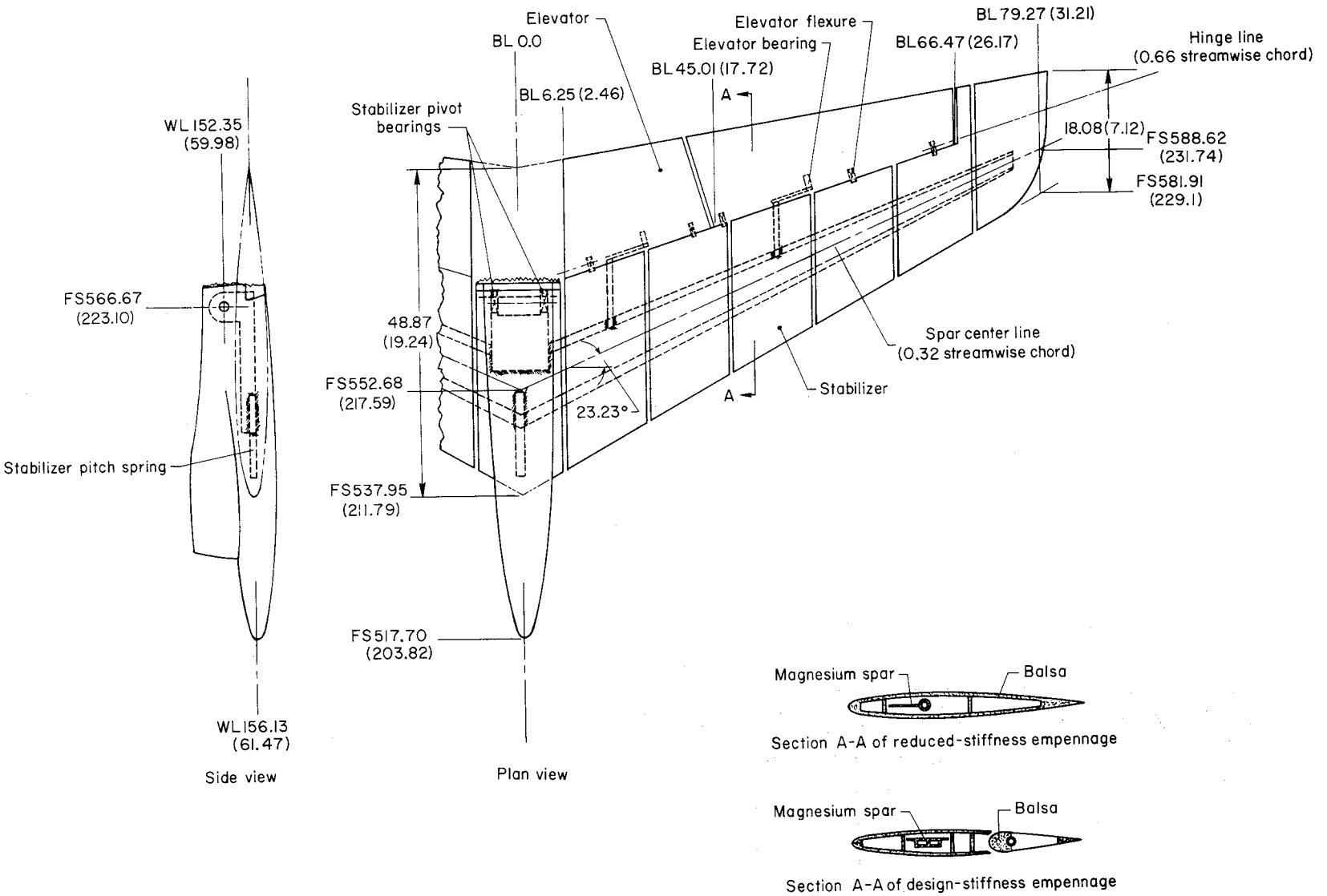

(b) Horizontal tail.

Figure 1.- Continued.

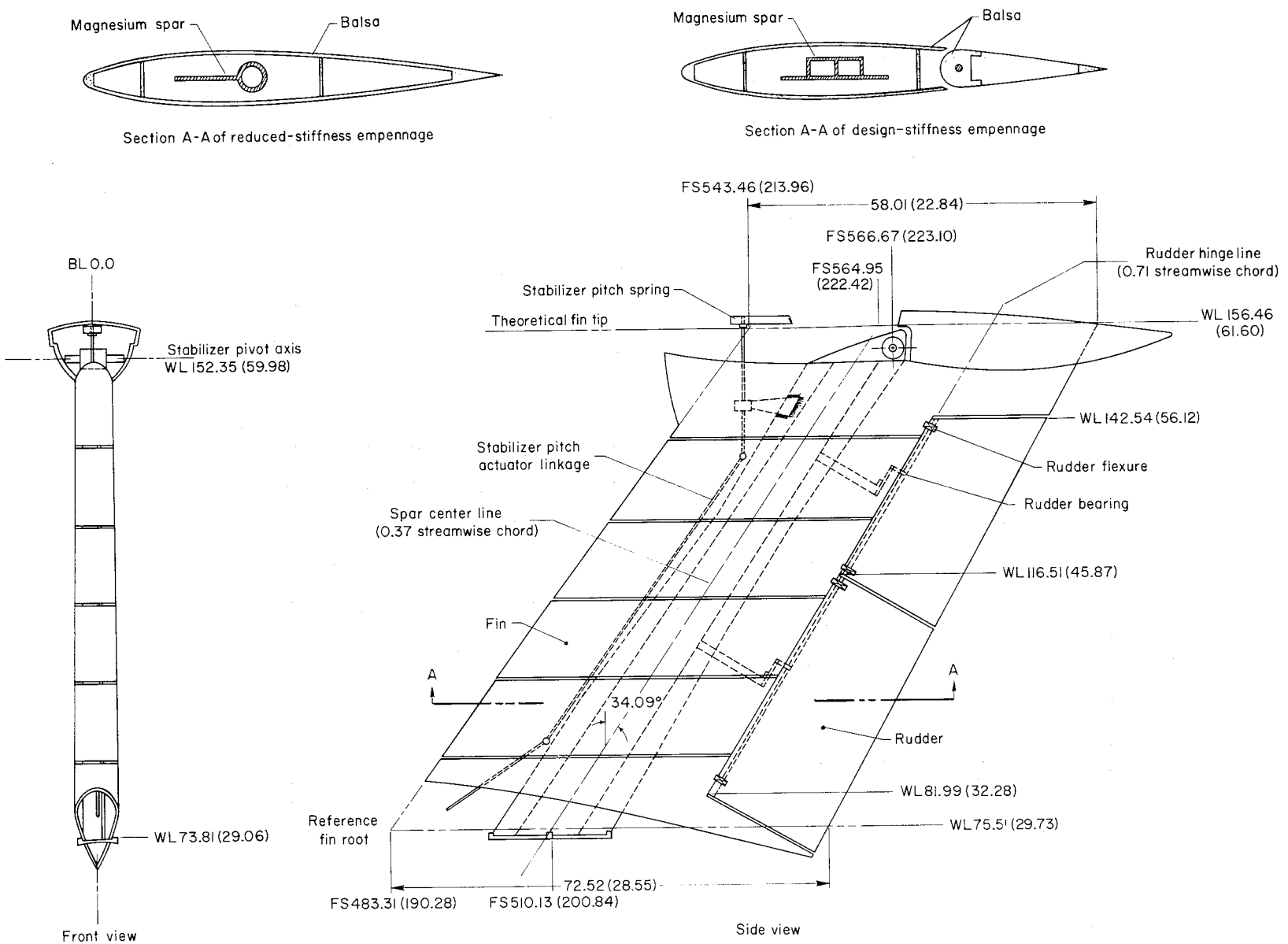

(c) Vertical tail.

Figure 1.- Continued.

Note:

Main support cables 1 and 2 lie in plane of symmetry and are inclined about 45° to horizontal. Cables are attached to springs located outside of test section.

Upper drag cables 3 and 4 are inclined 5° (wall attachment point up) to horizontal plane; lower drag cables 5 and 6 lie in horizontal plane. All drag cables are inclined 52.5° to plane of symmetry and are attached to tunnel walls.

Continous cable 7 lies in horizontal plane and is inclined 70° to plane of symmetry. Cable 7 passes between friction plates to provide damping in yaw.

Not shown are four snubber cables which are attached top and bottom to the front and aft end of the fuselage. The snubbers are used to restrain the model at the center line of the tunnel. The snubbers are normally slack during testing and were engaged in emergency situations.

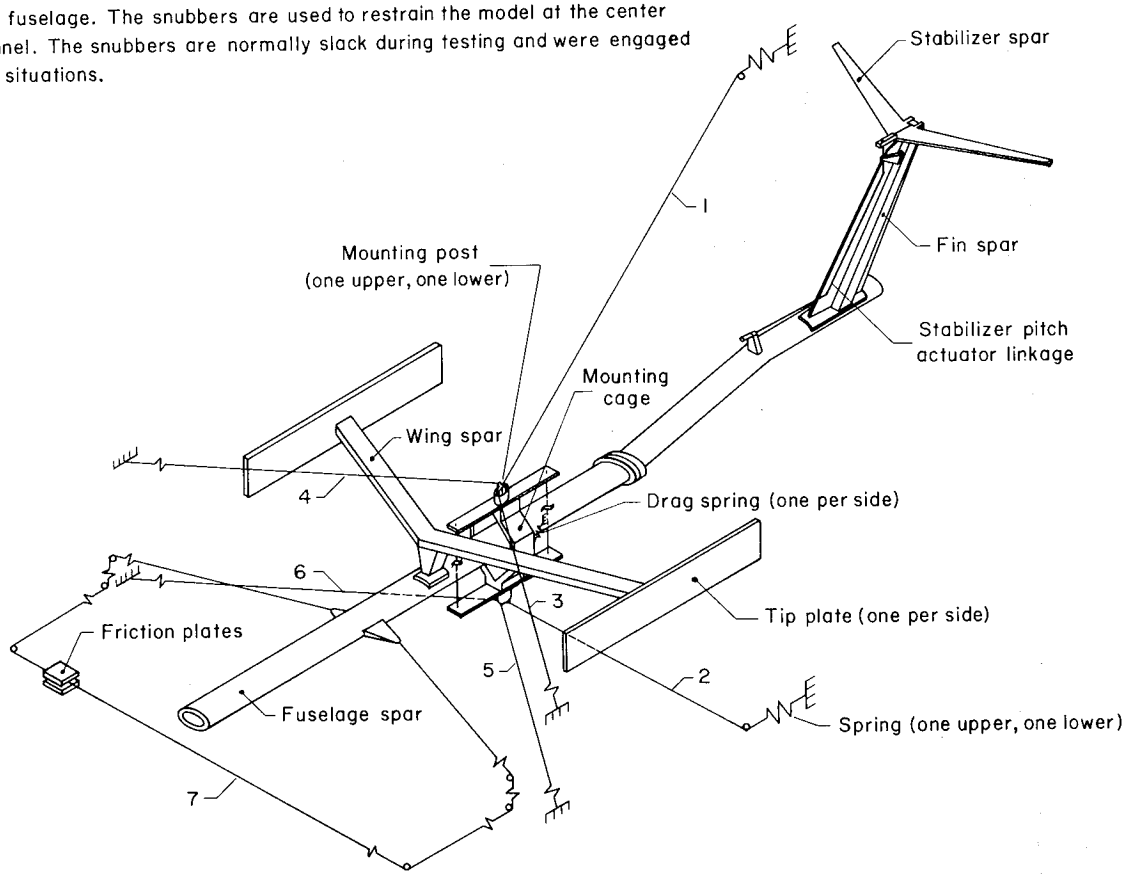

(d) Sketch showing main structural members of model and mount system.

Figure 1.- Concluded.

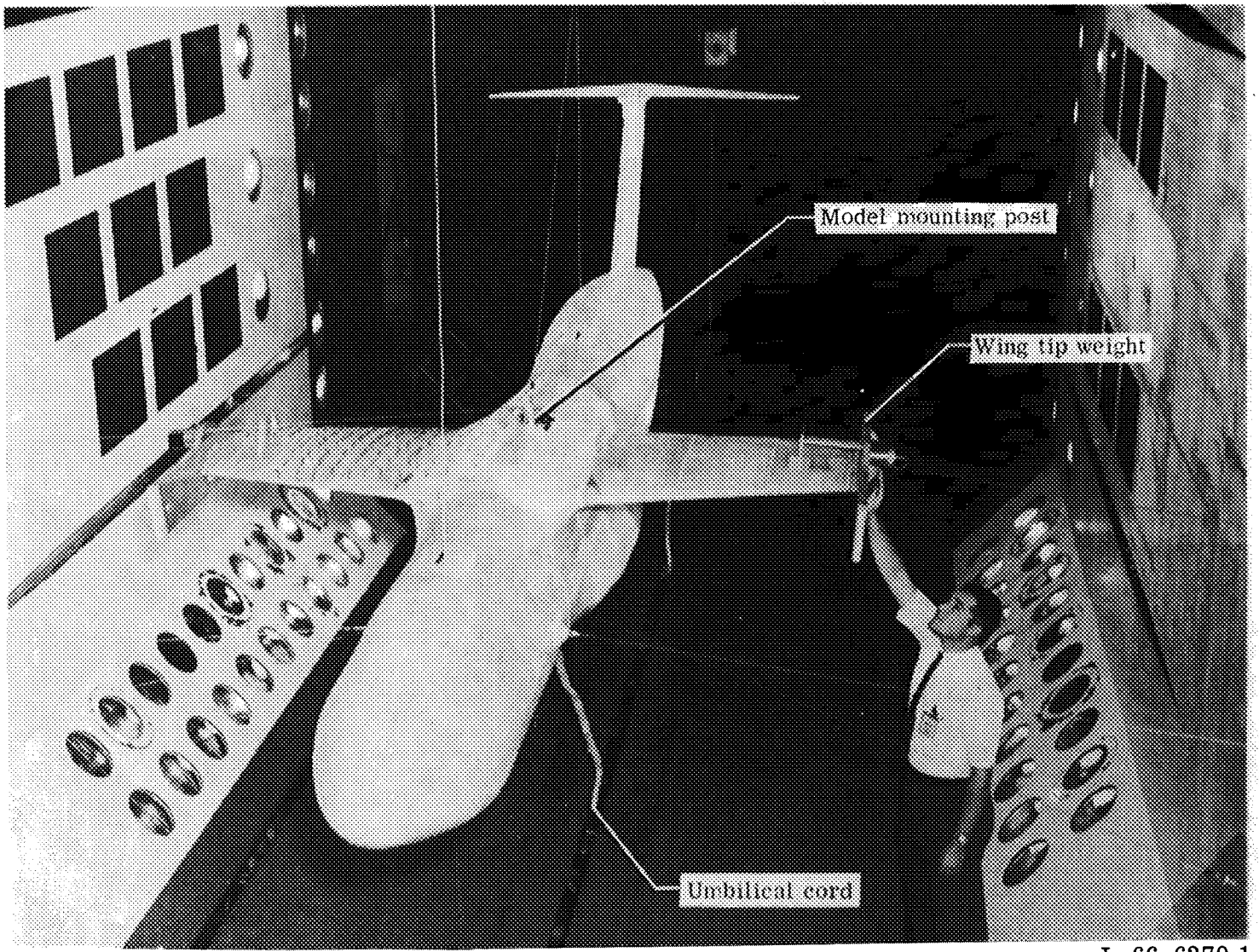

L-66-6270.1

(a) Model suspended in tunnel.

Figure 2.- Photographs of models.

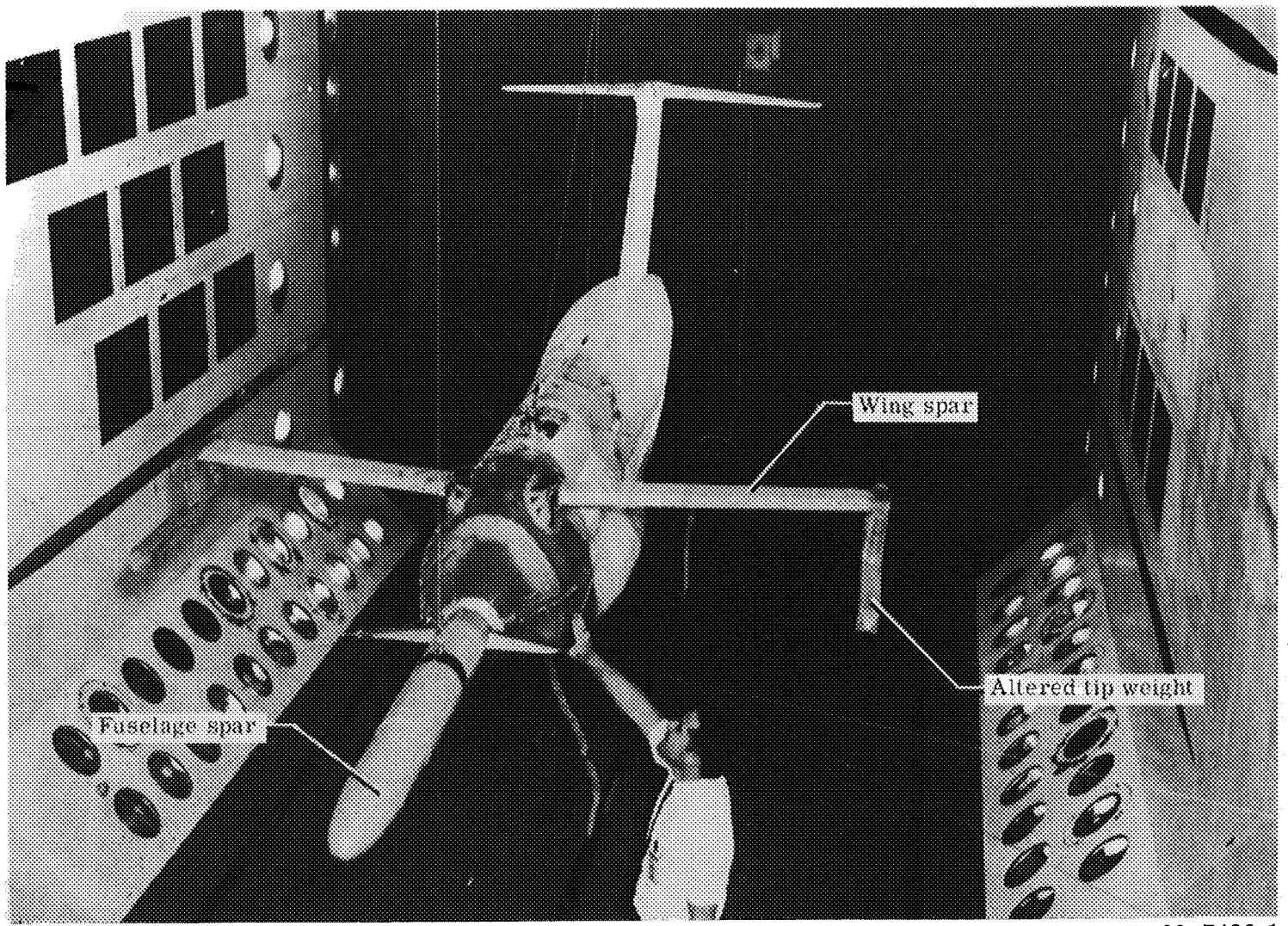

L-66-7429.1

(b) Model with altered wing shape and forward-fuselage shape.

Figure 2.- Continued.

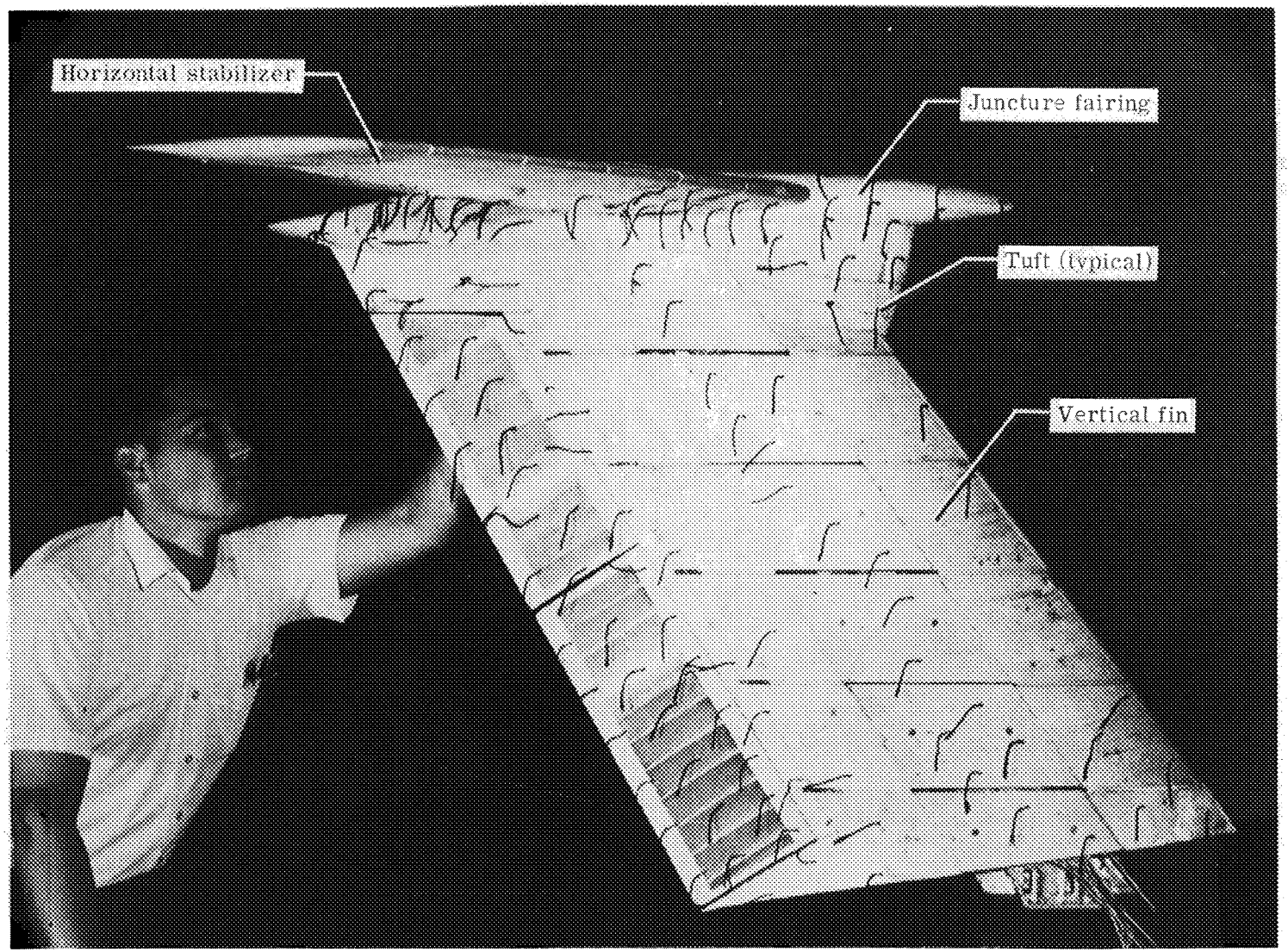

L-66-7463.1

(c) Design-stiffness empennage with nominal fin-stabilizer juncture fairing.

Figure 2.- Continued.

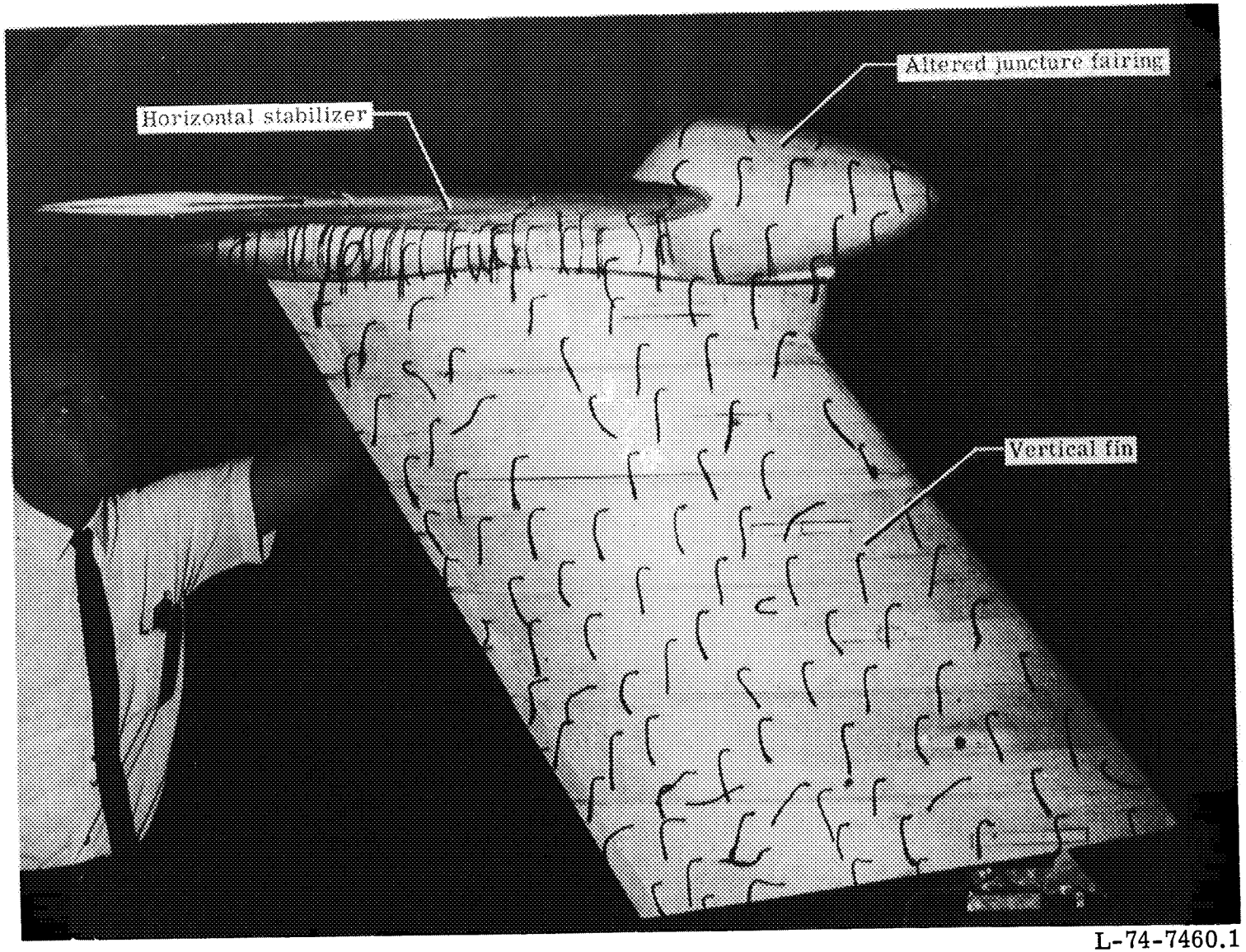

L-74-7460.1

(d) Reduced-stiffness empennage with altered fin-stabilizer juncture fairing.

Figure 2.- Concluded.

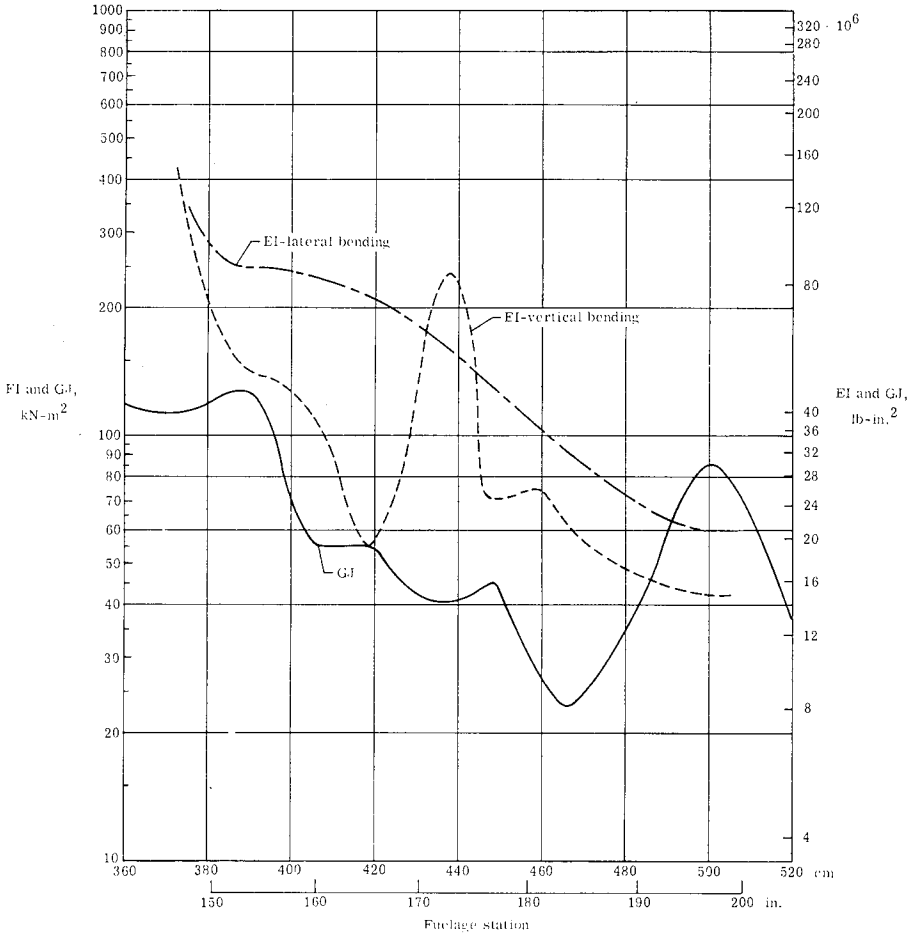

(a) Fuselage spar.

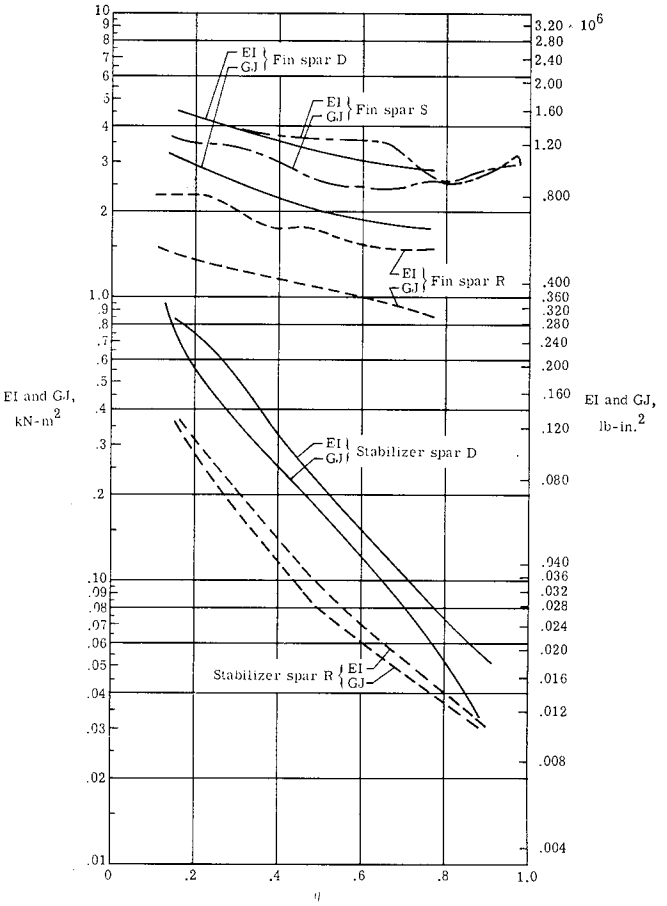

(b) Fin and stabilizer spars.

Figure 3.- Measured distributions of bending and torsional stiffnesses of fuselage, fin, and stabilizer spars.

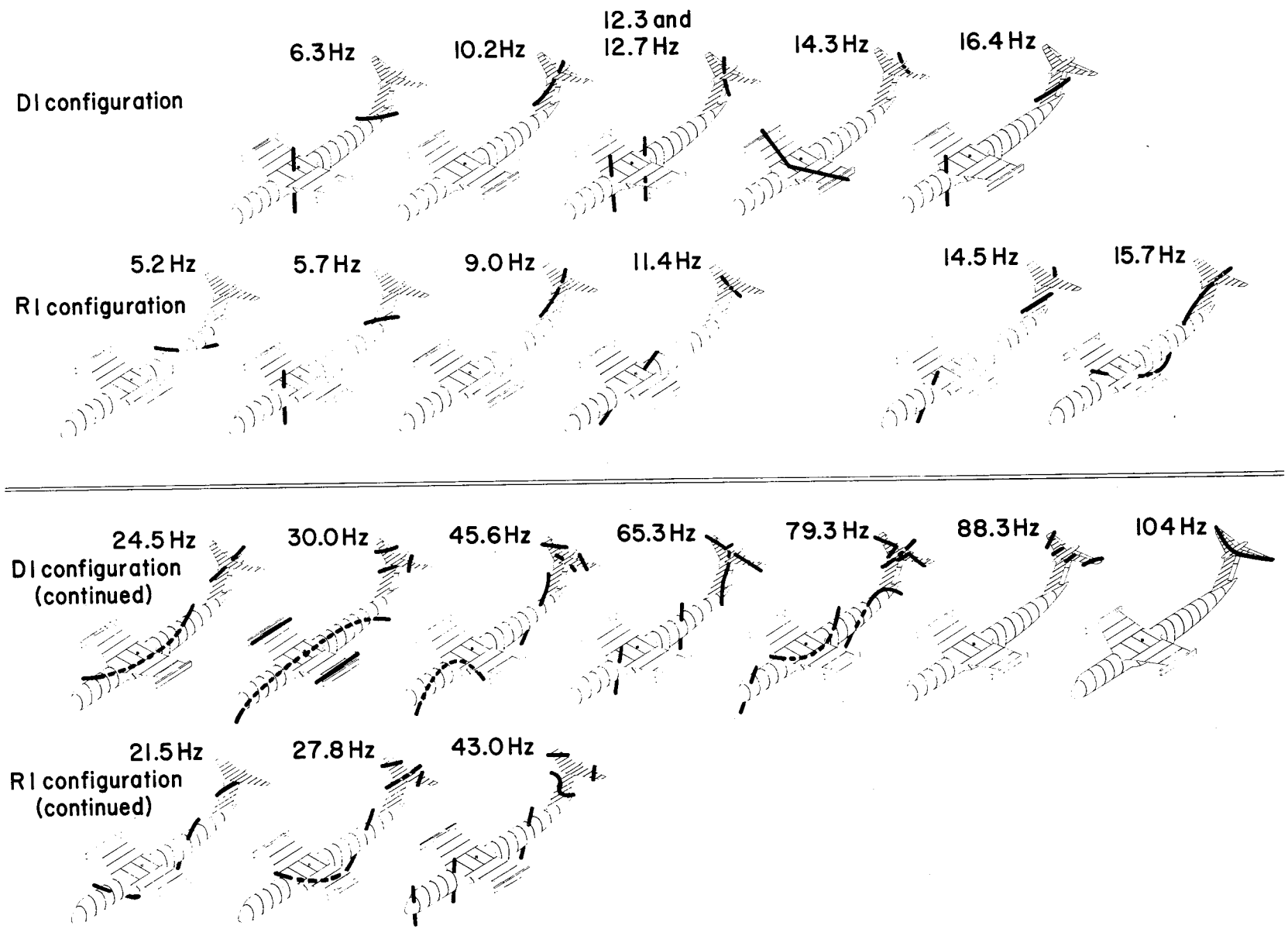

(a) Antisymmetric modes of complete-model configurations.

Figure 4.- Measured node lines associated with natural vibration frequencies for various model configurations.

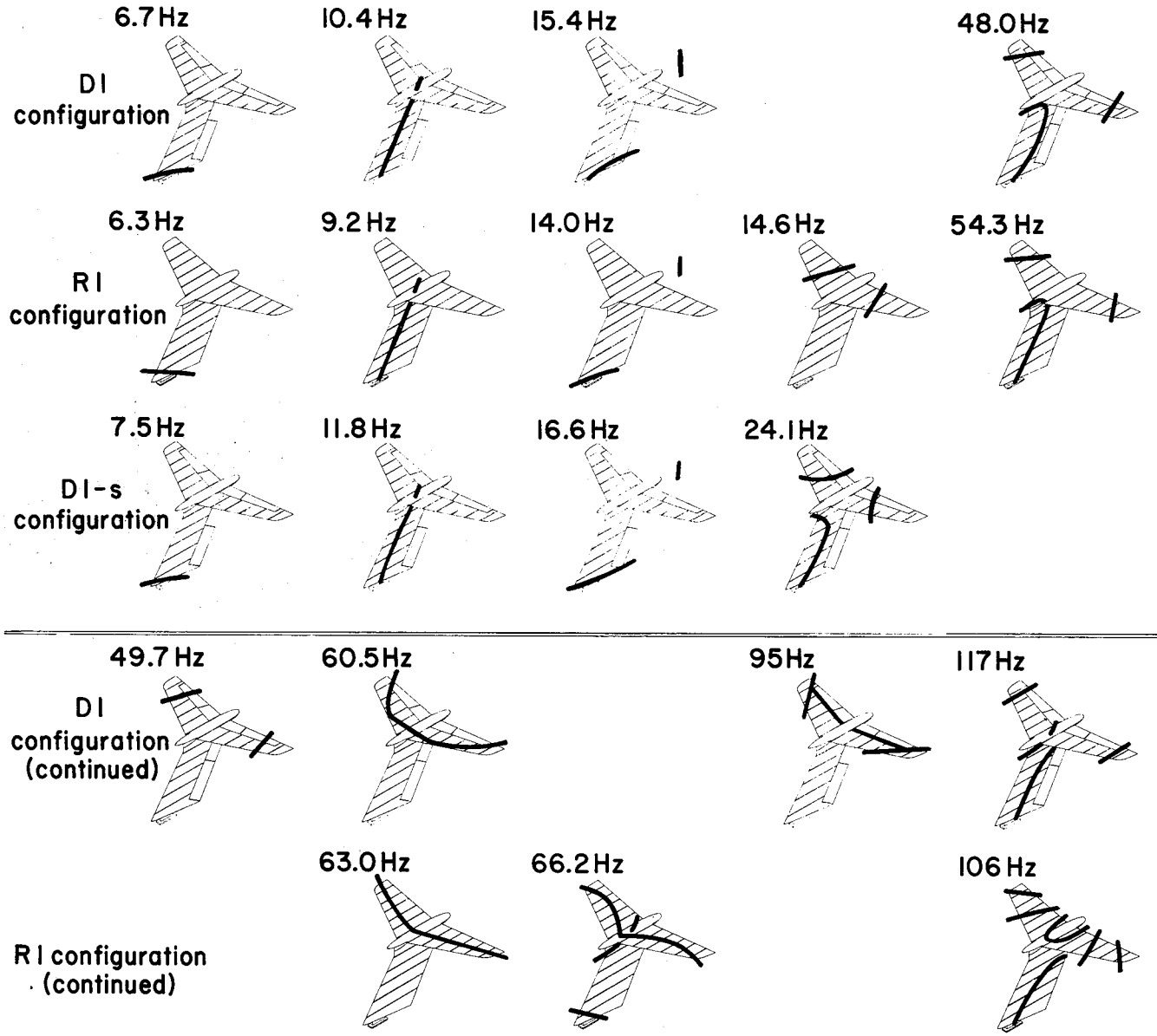

(b) Antisymmetric modes for model configurations cantilevered at fin root.

Figure 4.- Continued.

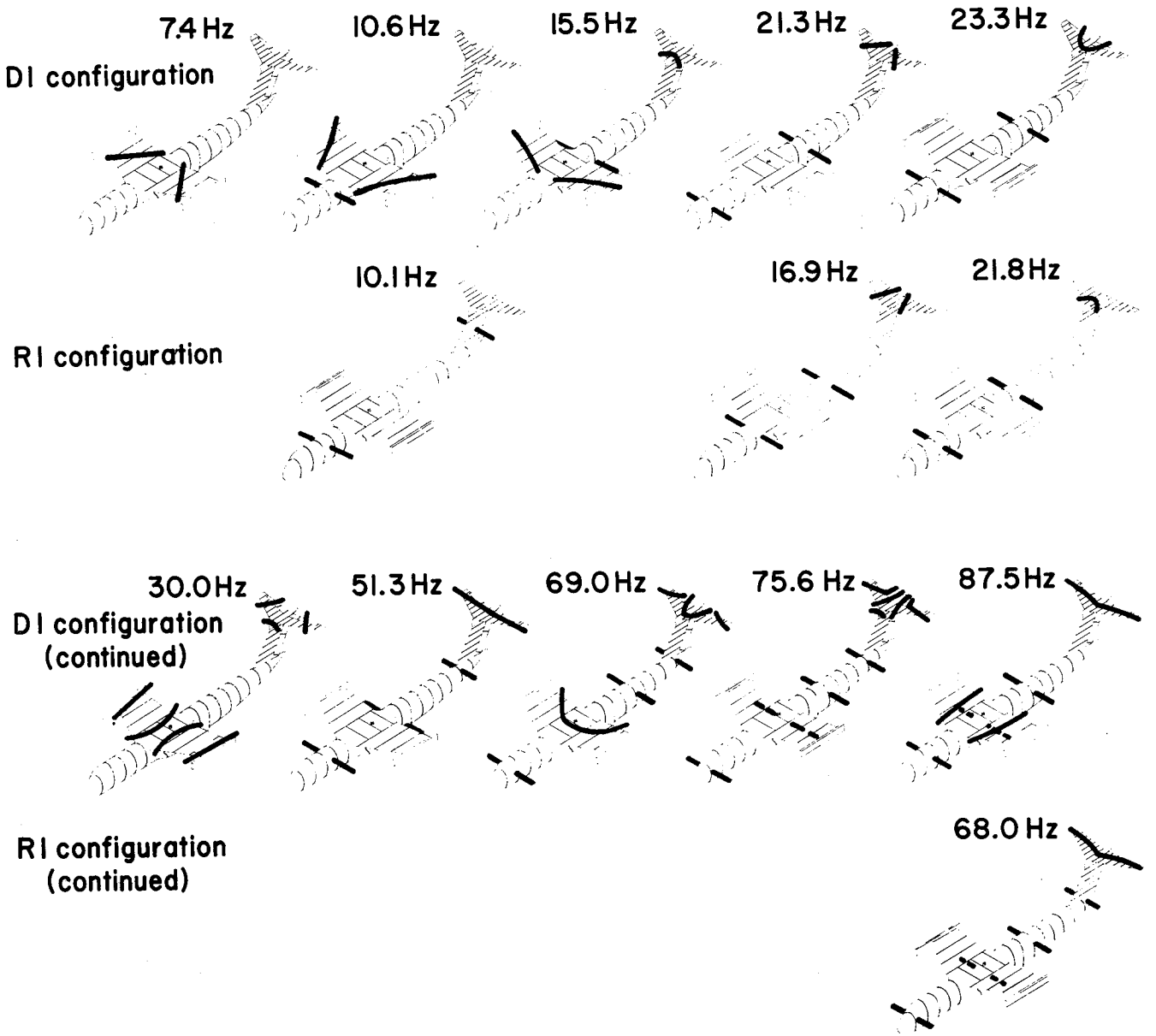

(c) Symmetric modes for complete-model configurations.

Figure 4.- Continued.

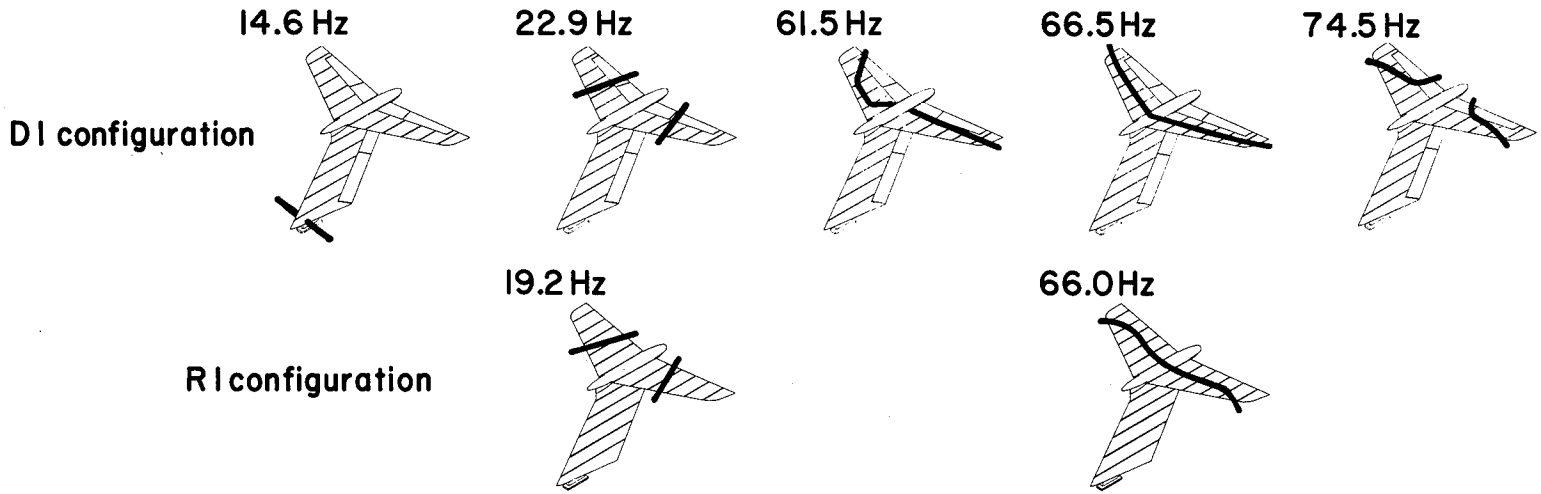

(d) Symmetric modes for model configurations cantilevered at fin root.

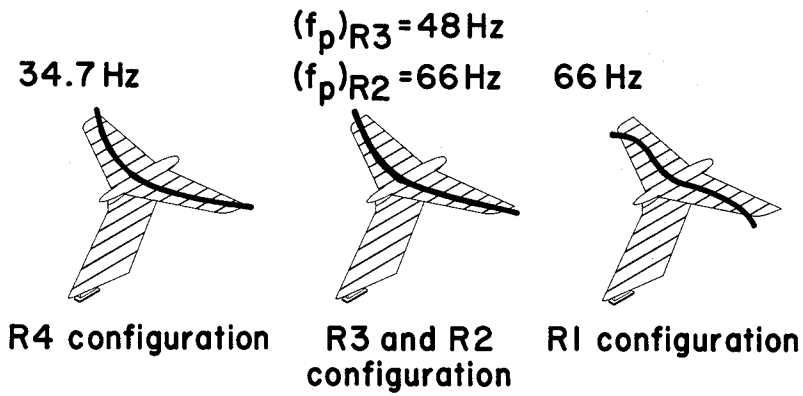

(e) Symmetric stabilizer pitch modes for various stabilizer pitch springs of configurations cantilevered at fin root.

Figure 4.- Concluded.

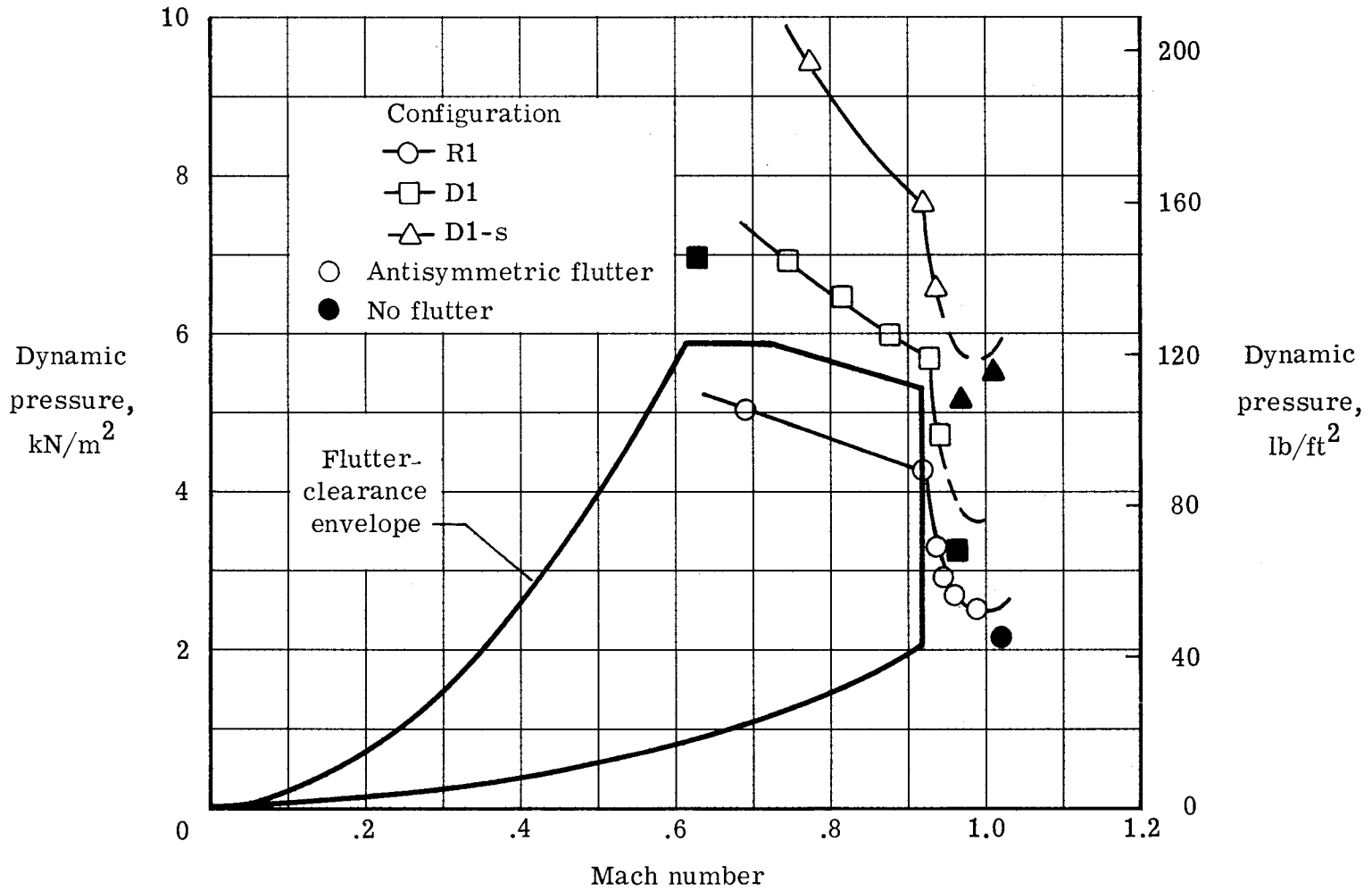

Figure 5.- Variation with Mach number of dynamic pressure required for antisymmetric flutter of basic empennage configurations.

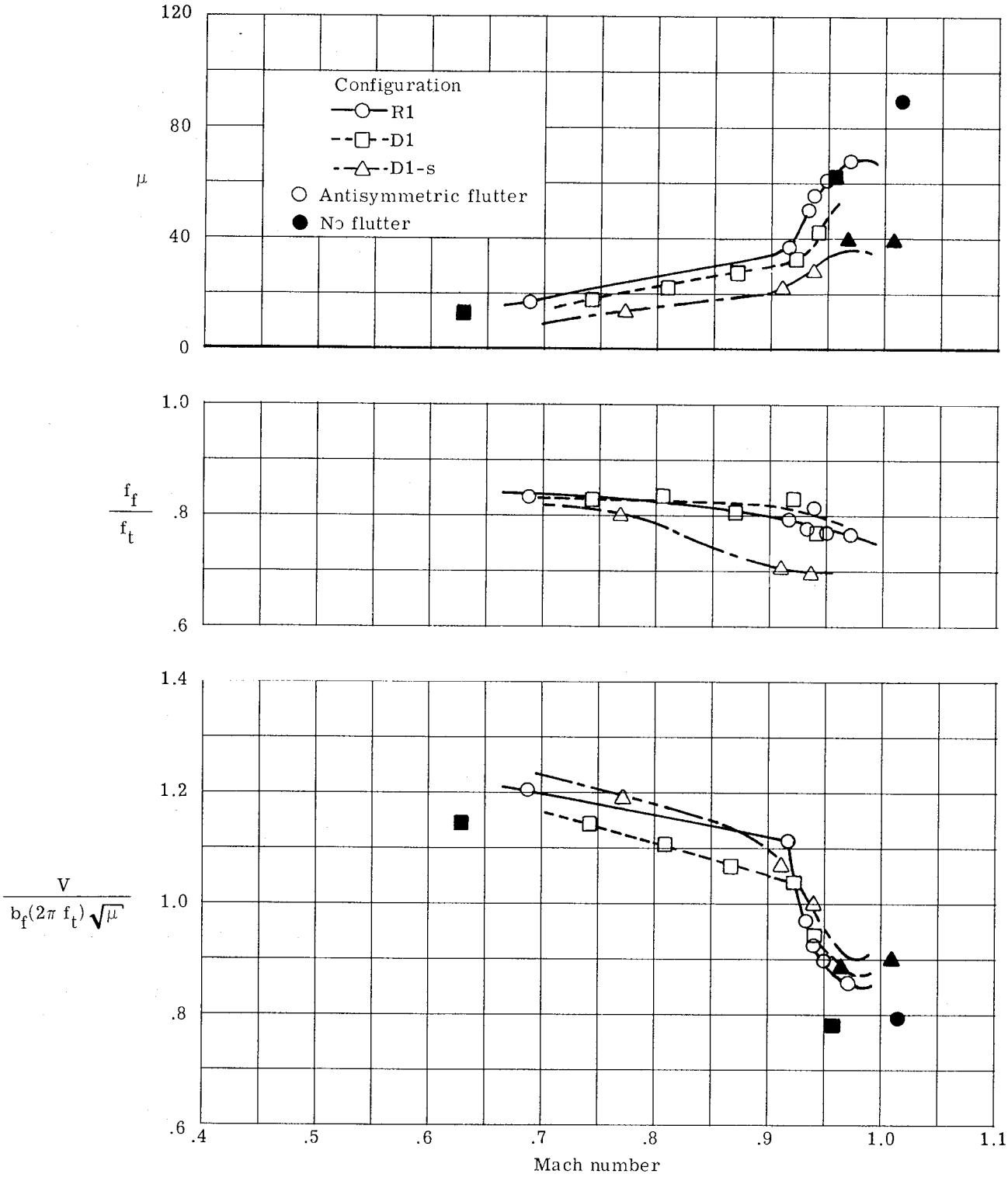

Figure 6.- Antisymmetric-flutter characteristics of basic empennage configurations.

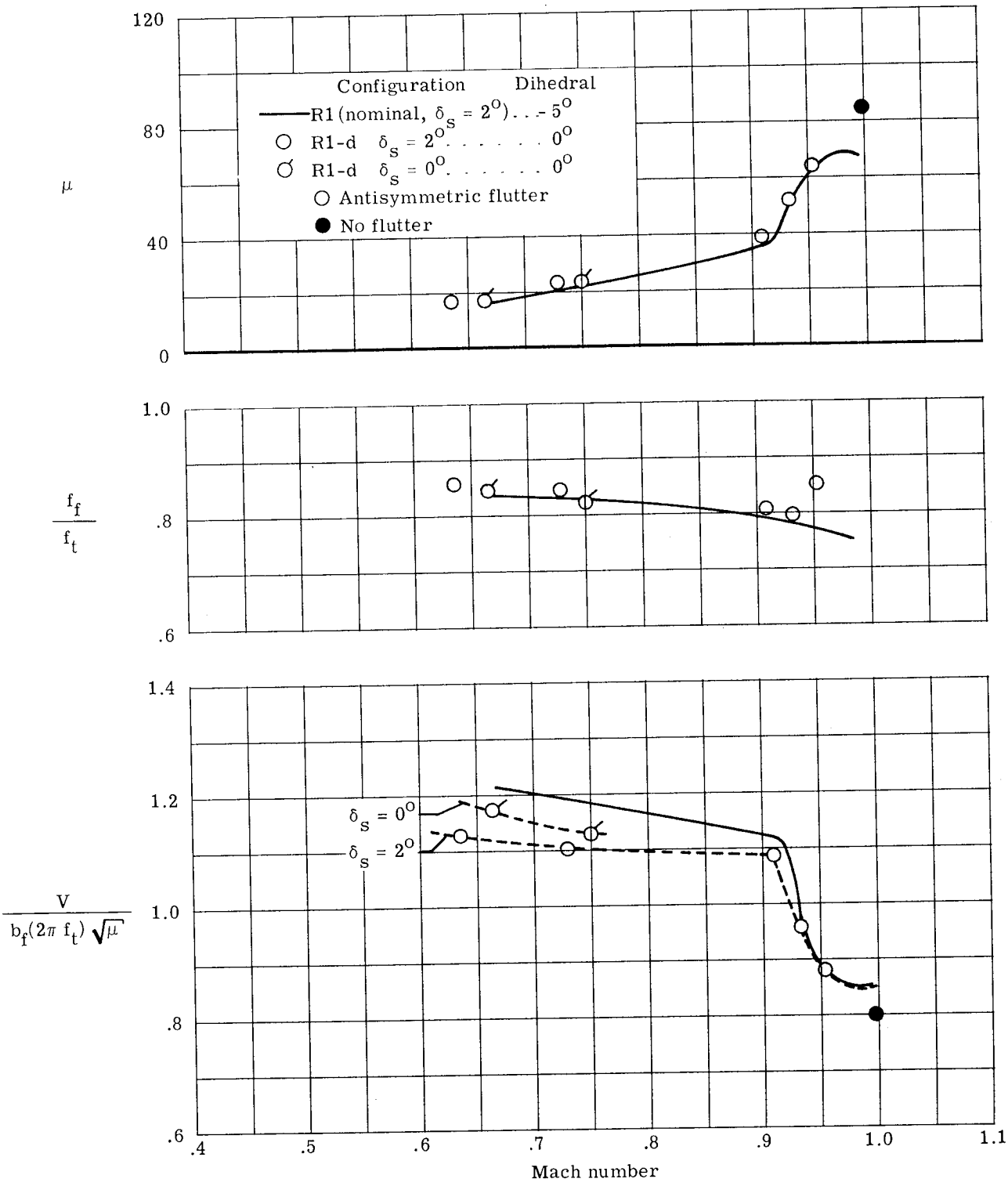

(a) Horizontal-tail dihedral and incidence angle.

Figure 7.- Parametric effects on the antisymmetric flutter of reduced-stiffness configurations.

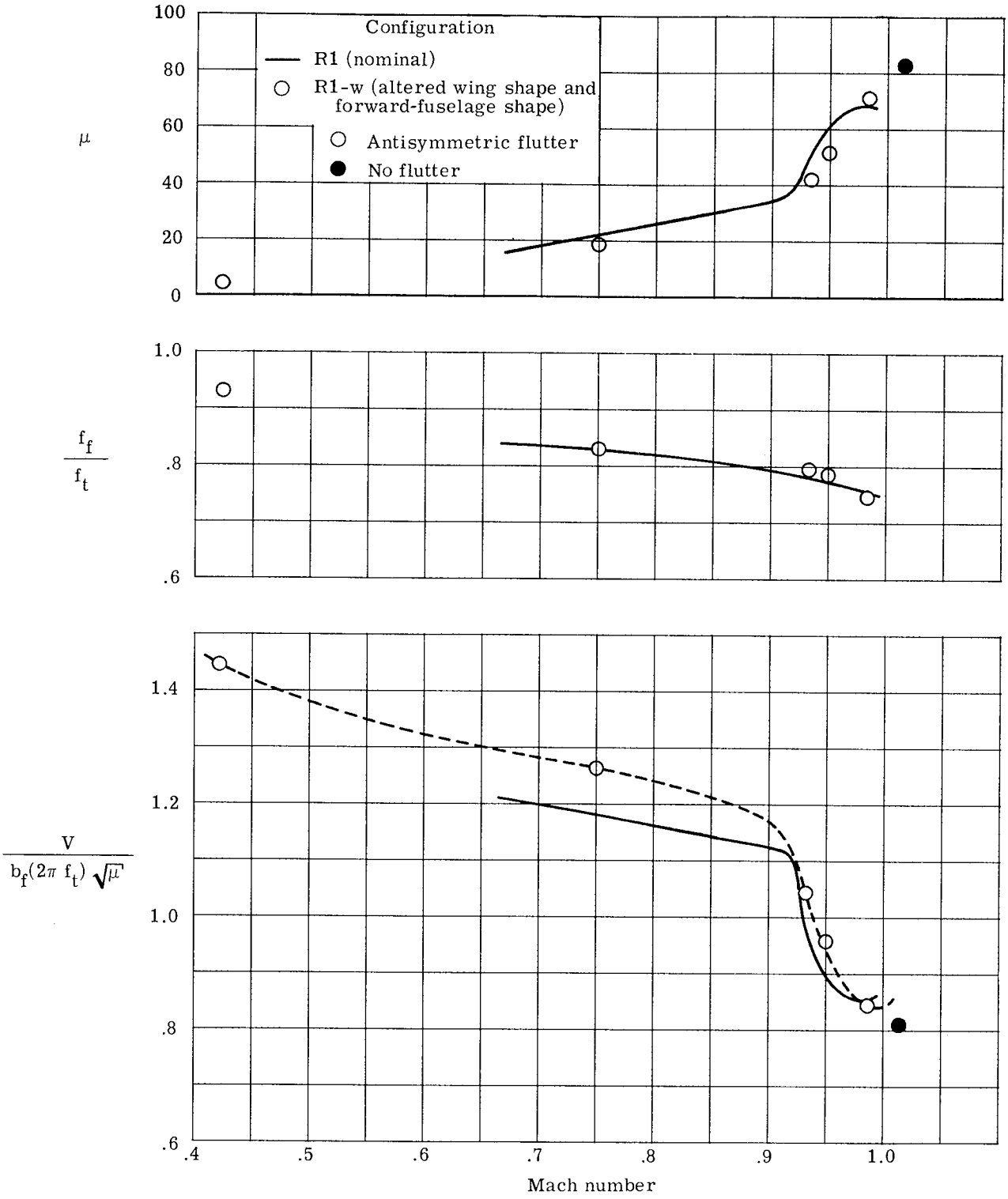

(b) Altered wing shape and forward-fuselage shape.

Figure 7.- Continued.

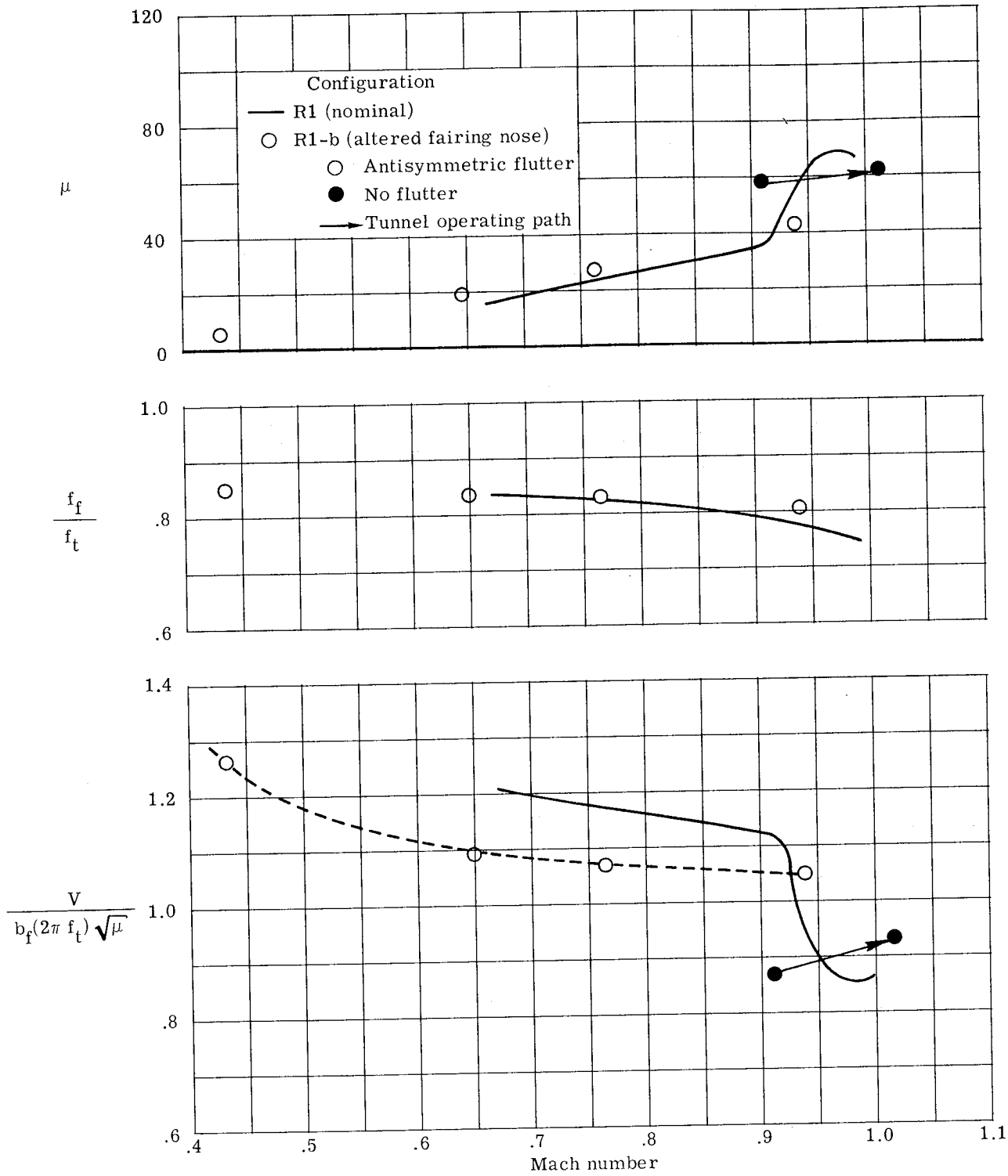

(c) Altered nose shape of fin-stabilizer juncture fairing.

Figure 7.- Concluded.

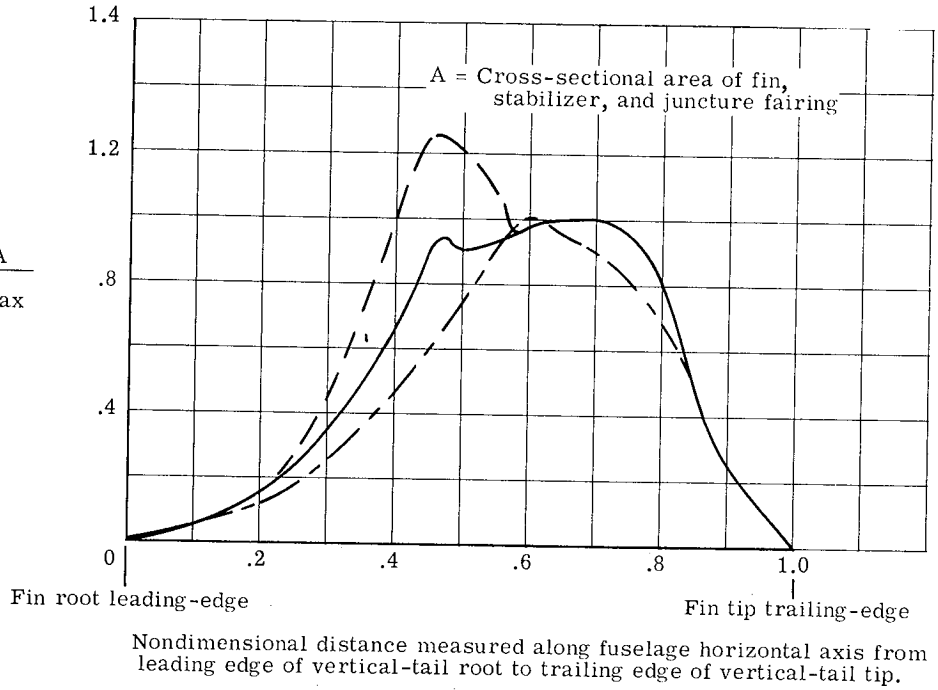

(a) Empennage cross-sectional area distribution.

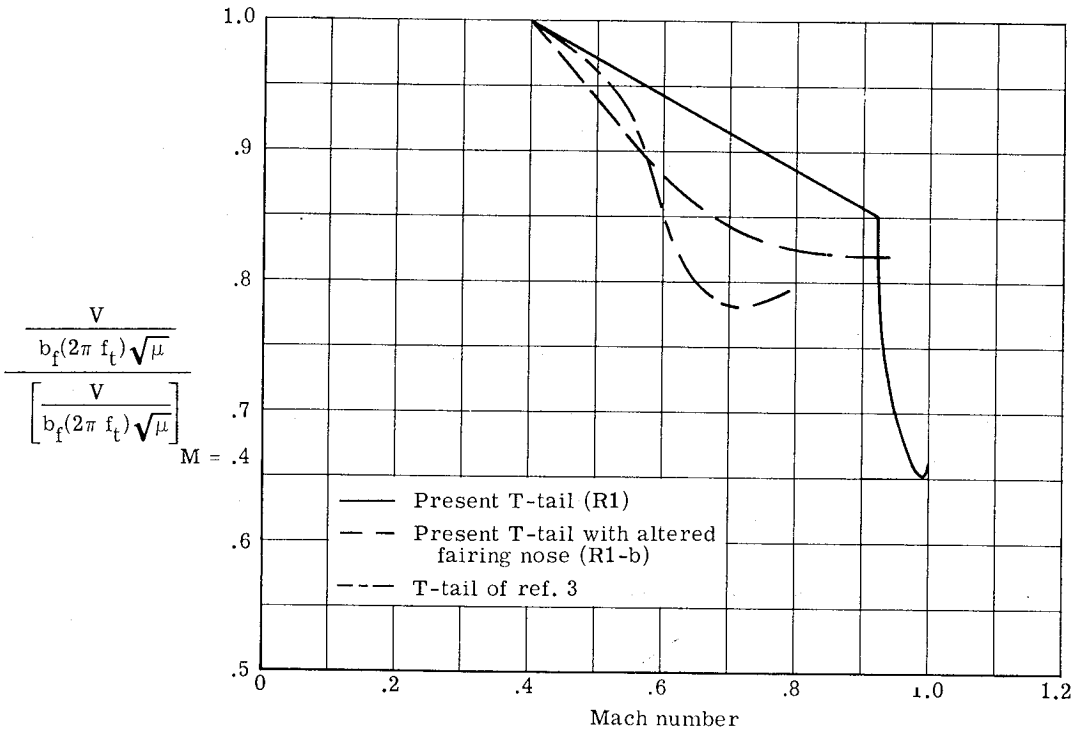

(b) Variation of normalized antisymmetric-flutter-speed index with Mach number.

Figure 8.- Comparison of transonic-antisymmetric-flutter boundaries and empennage area distributions of present T-tail models and T-tail model of reference 3.

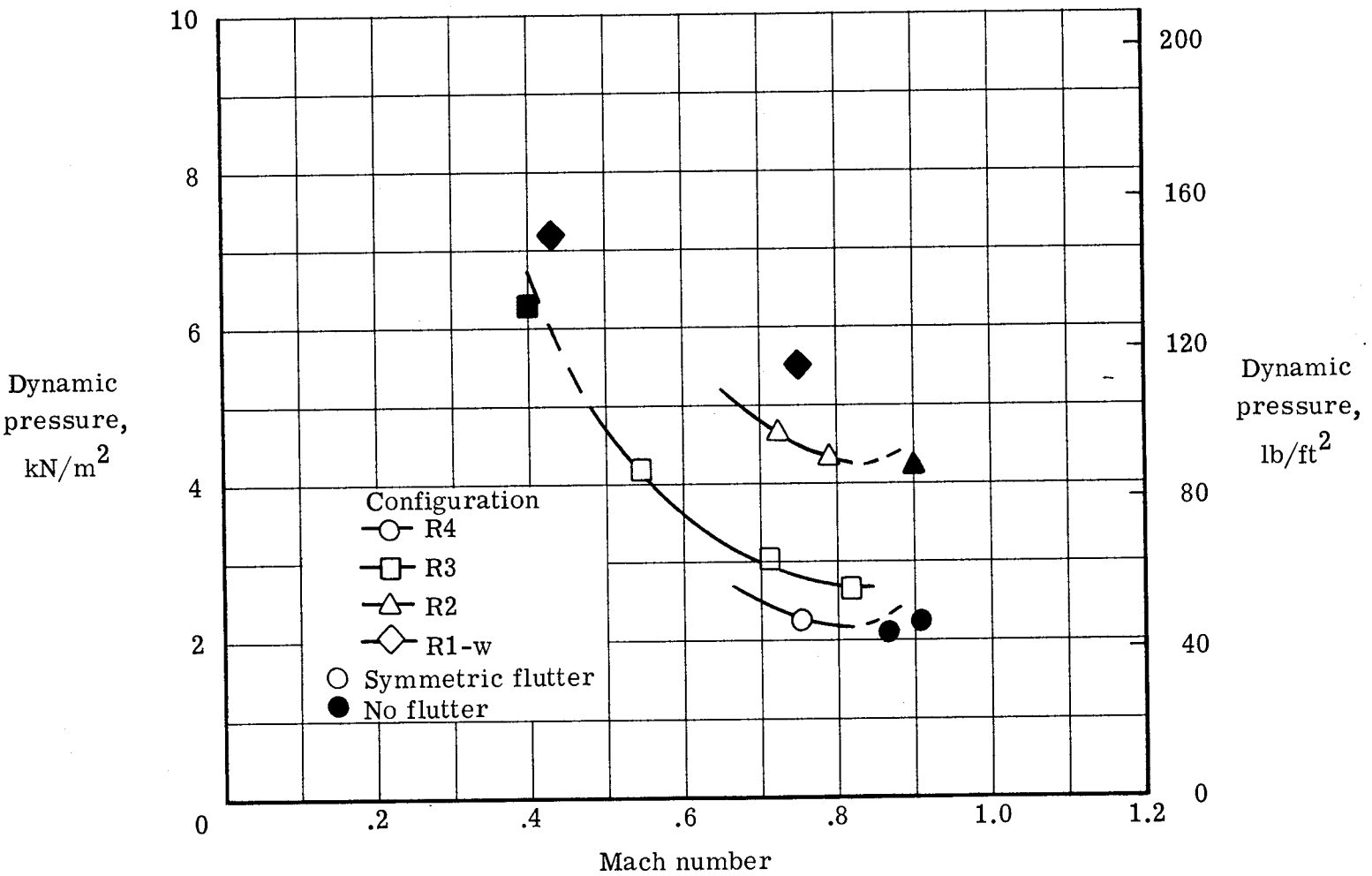

Figure 9.- Variation with Mach number of dynamic pressure required for symmetric flutter of reduced-stiffness configurations.

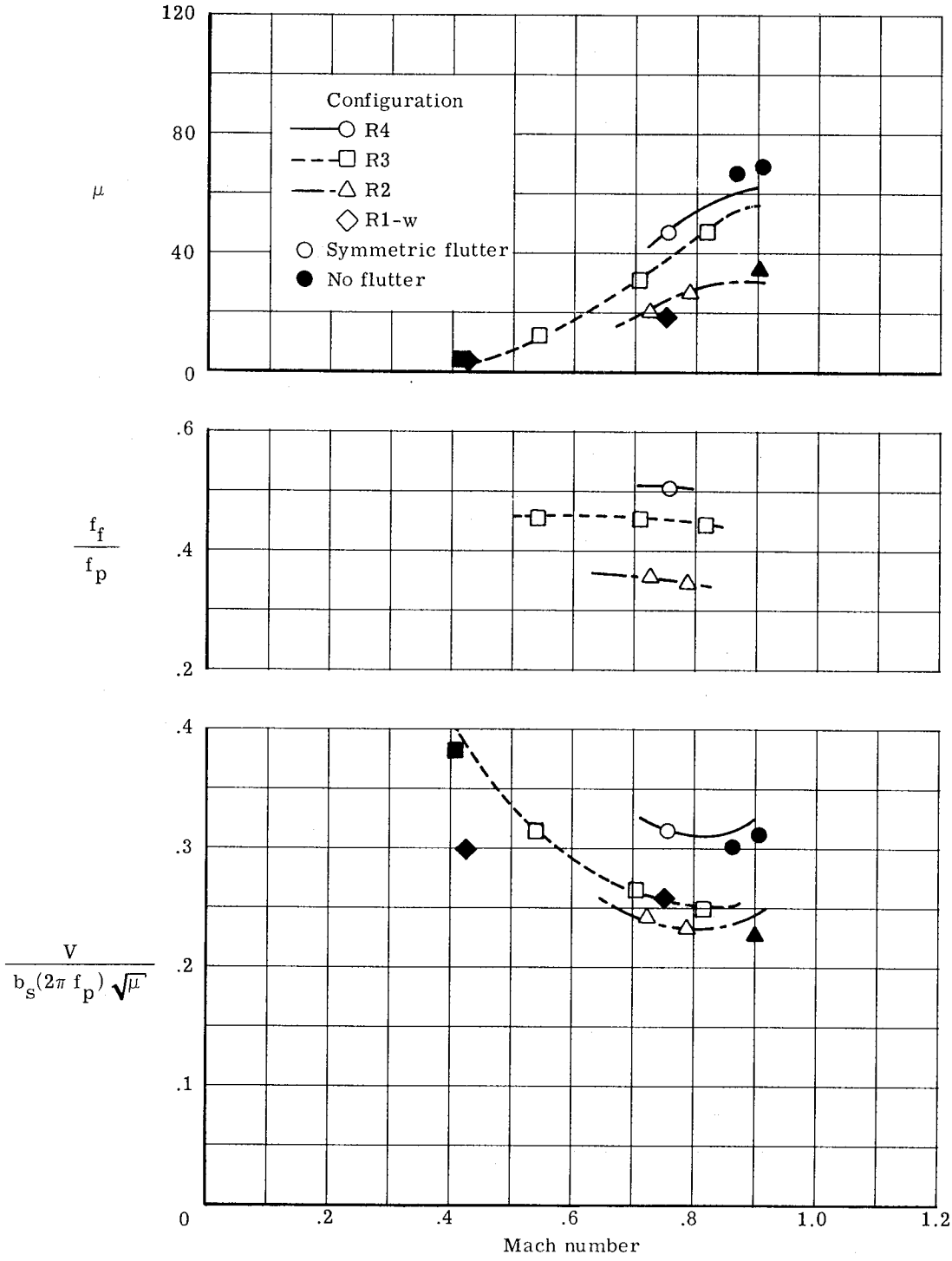

Figure 10.- Symmetric flutter characteristics of reduced-stiffness model with various stabilizer pitch springs.

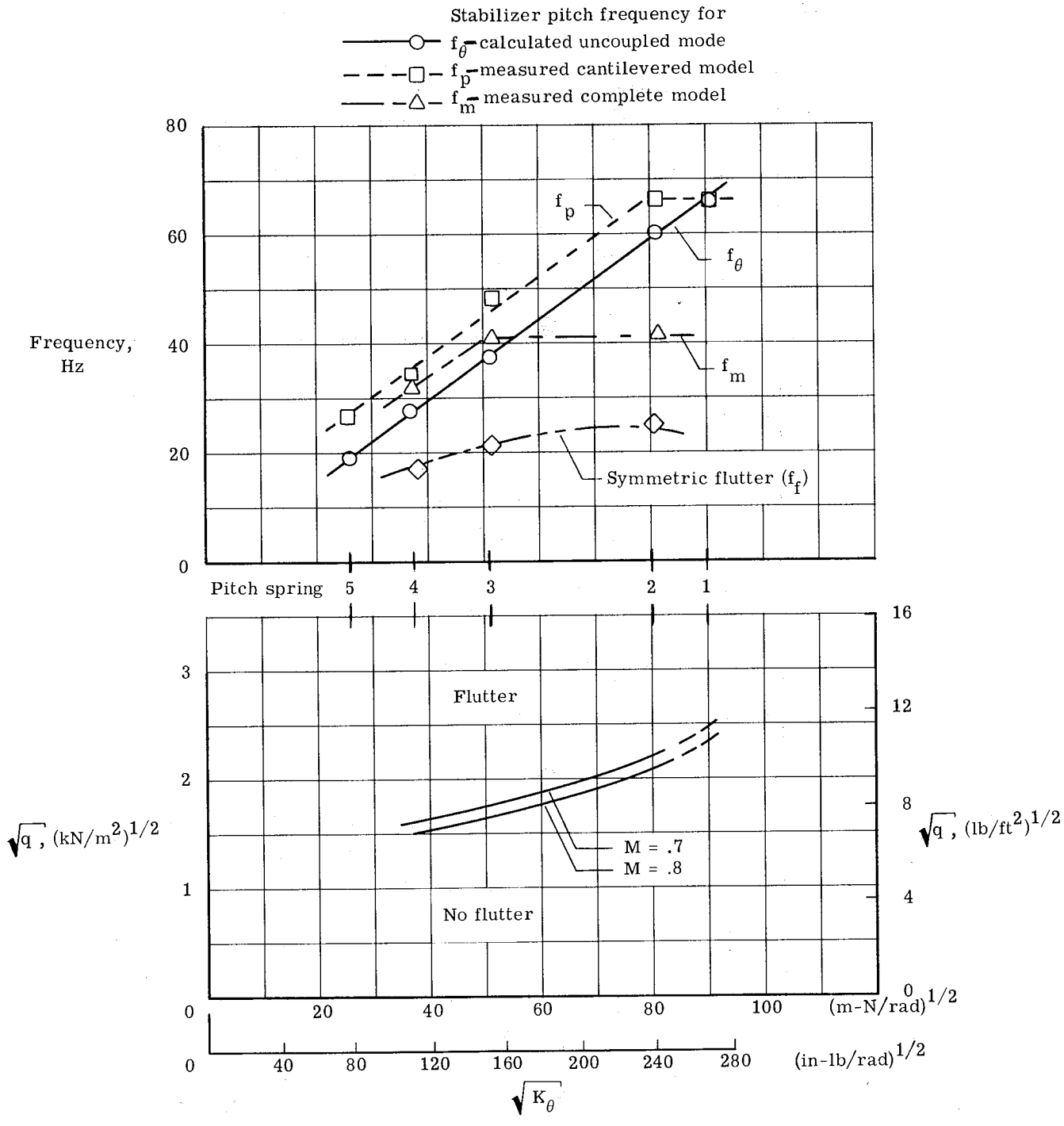

Figure 11.- Effect of stabilizer-pitch-spring stiffness on symmetric-flutter dynamic pressure and related frequencies of reduced-stiffness model.